DFT Quantum Chemical Calculations and Statistical Analysis of 2-Amino-6-arylsulfonylbenzonitrile Derivatives and their Electrical Properties

[1]M. Izzettin Yilmazer, [1]Murat Saracoglu*, [2]Murat Alper Basaran, [3]Hakan Sezgin Sayiner, [4]Fatma Kandemirli
[1]*Erciyes University, Faculty of Education, 38039, Kayseri, Türkiye. Email: izzettin@erciyes.edu.tr ; muratsaracoglu@gmail.com*
[2]*Alanya Alaaddin Keykubat University, Faculty of Engineering, 07425, Antalya, Türkiye. Email: murat.basaran@alanya.edu.tr*
[3]*Adıyaman University, Faculty of Medicine, 02200, Adıyaman, Türkiye. Email: drhssayiner@yahoo.com*
[4]*Kastamonu University, Faculty of Engineering and Architecture, 37150, Kastamonu, Türkiye. Email: fkandemirli@yahoo.com*

*Corres. Author: muratsatracoglu@gmail.com**

(Received on 12th September 2025, accepted in revised form 23rd January 2026)

Summary: Quantum chemical calculations were performed for gas and water phases using the DFT/B3LYP/6-311G(d,p) basis set to determine some molecular properties of 2-amino-6-arylsulfonylbenzonitrile derivatives (1-61). The quantum chemical properties of these compounds such as E_{HOMO} (highest occupied molecular orbital energy), E_{LUMO} (lowest unoccupied molecular orbital energy), HOMO-LUMO energy gap (ΔE), ionization potential (*I*), chemical hardness (η) and softness (σ), etc. values were calculated and the results were discussed. This research aims to construct the relationship between HIV-reverse transcriptase inhibitory activity (pIC_{50}) values and classical-quantum descriptors (attributes) of 61 compounds. The values of the attributes are extracted by utilizing B3LYP/6-311G(d,p) method. This endeavour leads to different statistical models since the data contain both nonlinearity and clustered structure. In this study, 2-amino-6-arylsulfonylbenzonitrile derivatives (1-61) were classified into three subsets based on the atom or group attached at the X position: Subset S (compounds 1-19), Subset SO (compounds 20-32), and Subset SO_2 (compounds 33-61). Then each subgroup is split into more statistically homogeneous subsets using statistical models suggesting that the ratio denoted by $\frac{\Delta E}{I}$ is the most significant variable that accounts for pIC_{50} for both groups of S and SO_2 with 95 and 90 percent coefficients of determination, respectively. On the other hand, for the group SO, we have a more complicated significant variable that accounts for pIC_{50}, which is $\frac{I+DM}{EN*Electrophily}$.
Moreover, In the context of 2-amino-6-arylsulfonylbenzonitrile derivatives, compounds **2**, **24**, and **50** for gas phase, and compounds **15**, **30**, and **50** for water phase exhibit higher HOMO energies and smaller ΔE values compared to other molecules in the series. This suggests that, according to the ΔE values, these compounds have a higher tendency to donate electrons and have a more effective reactivity than the other compounds in the series.

Keywords: 2-Amino-6-arylsulfonylbenzonitrile derivatives; DFT; Quantum chemical calculations; Statistical analysis.

Introduction

Human Immunodeficiency Virus (HIV) damages cells that help the body fight infection, making people more vulnerable to other infections and diseases [1]. HIV is divided into two subtypes: HIV-1 and HIV-2. While these are quite similar in their replication mechanisms and transmission routes, HIV-1 infections have been found to progress more rapidly than HIV-2 infections [2, 3]. HIV-1 is the primary cause of AIDS, which poses a serious threat to public health worldwide [1, 2, 4]. It is estimated that 39.9 million people worldwide will be living with HIV in 2023. Of these, 38.6 million were adults over the age of 15, and 1.4 million were children under the age of 15. 53% of these people are women and girls. Additionally, an estimated 630,000 people worldwide will die from AIDS in 2023. Once HIV enters the human body, you have HIV for life. Although the treatments used to treat HIV do not eliminate HIV in the blood, they can reduce it to very low levels where a person can live a healthy life [1].

Various series of compounds are being studied as inhibitors against HIV. One of these series is the 2-amino-6-arylsulfonylbenzonitrile derivatives reported by Chan et al. [5]. Studies are showing that 2-amino-6-arylsulfonylbenzonitrile derivatives are used as anti-HIV-1 activity [3, 5-9]. Roy and Leonard studied the anti-HIV-1 activity of 2-amino-6-arylsulfonylbenzonitriles

*To whom all correspondence should be addressed.

and their thiol and sulfinyl derivatives using their binding affinities, physicochemical and quantum chemical parameters using multiple regression techniques with factor analysis [6]. However, these studies lacked a comprehensive quantum-chemical and statistical analysis of the electronic properties governing their inhibitory activity. Our work bridges this gap by employing DFT calculations and advanced statistical modelling to correlate quantum descriptors with pIC50 values, providing a deeper understanding of the structure-activity relationship (SAR) for these compounds. Hu et al. performed molecular modelling of the same series using comparative molecular field analysis (CoMFA) and comparative molecular similarity index analysis (CoMSIA) approaches to determine the most probable binding mode and reliable conformations [7].

Quantitative Structure-Activity Relationship (QSAR) is a method that examines the relationship between various physical parameters and the biological activities of compounds. QSAR methods have been successfully used for the prediction of the activities of various drugs and drug-like compounds for a long time and have made great contributions to computer-aided drug design. QSAR is based on the approach that changes in the structure of compounds are associated with changes in their molecular properties. For this purpose, three-dimensional QSAR (3D-QSAR), CoMFA and CoMSIA models are widely used in studies together with statistical approaches such as Multiple Linear Regression (MLR), Partial Least Squares (PLS) and Artificial Neural Networks (ANN) [10-15]. In this study, 2-amino-6-arylsulfonylbenzonitrile and their thiol and sulfinyl derivatives (1–61) [9] were examined into three subsets based on the substituent at the X position: Subset S (benzonitrile derivatives): Compounds 1–19, Subset SO (thiol derivatives): Compounds 20–32, Subset SO_2 (sulfinyl derivatives): Compounds 33–61 (Table-1). To ensure the robustness and predictive capability of our models, we have considered the importance of external validation. While our internal validation using 5-fold cross-validation yielded high accuracy (91.8%), future studies would benefit from applying these models to an independent dataset to confirm their predictive power, as emphasized in QSAR best practices [16, 17].

The molecules were optimized using the Gaussian 09 (revision A.02 [18]) program with the DFT/B3LYP/6-311G(d,p) basis set. Quantum chemical parameters such as; the energy of E_{HOMO} (the highest occupied molecular orbital energy), E_{LUMO} (the energy of the lowest unoccupied molecular orbital energy), HOMO-LUMO energy gap (ΔE), ionization potential (I), chemical hardness (η) and softness (σ), electronegativity (χ) for gas and water phases were calculated, and the relationship between the activity and stability of the molecules of these results were discussed. Recently, the optimization of the molecules by using different basic sets and the discussion of the results have been widely used [19-36]. In addition, the relationship between the structures of the molecules and their reactivity, pIC50 values, was tried to be explained with the help of QSAR [37]. Also, statistical analysis of those 61 molecules is conducted to explain relations between pIC_{50} and quaquantum descriptor variables. The results suggest that intrinsically nonlinear relations in 3 statistically verified (R^2=0.92) subgroups exist. Besides, each subgroup is split into statistically verified subsets that contain molecules, which brings a new perspective to comprehending relations between pIC_{50} quantum descriptor variables. Instead of having a single set of descriptor variables accounting for relation, a constructed variable containing a ratio of combination of descriptor variables is found.

Parameters such as HOMO-LUMO enrgy gap, electronegativity and dipole moment, which are important in drug interactions, also affect the adsorption behavior of molecules on metal surfaces in corrosion inhibition. Drugs and corrosion inhibitors generally follow similar adsorption mechanisms, forming protective layers on surfaces through physical or chemical adsorption. Quantum chemical parameters are important in understanding interactions in both pharmacology and corrosion science. Functional groups such as amines, heterocycles, and π-electrons play significant roles in these donor-acceptor interactions.

Some authors agree that the drugs can be used well as corrosion inhibitors that can be complemented positively with a green corrosion inhibitor since most drugs and medicines are derived from natural substances [38-42]. The fact that the APIs molecule contains oxygen, nitrogen, and sulfur as an active center and the APIs are environmentally friendly and important in biological reactions supports the use of APIs as corrosion inhibitors. Biologically active molecules have been reported as good corrosion inhibitors. In addition, many expired drugs have been reported to be quite effective corrosion inhibitors for the preservation of soft steel in an acidic environment [43, 44].

Table-1: Chemical structures of investigated 2-amino-6-arylsulfonylbenzonitrile and their thiol and sulfinyl derivatives [9].

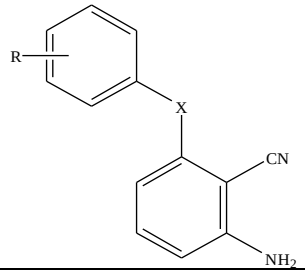

Comp.	Subset	X	R	Ref.	Comp.	Subset	X	R	Ref.
1	S	S	H	[9]	32	SO	SO	3-OCH_3, 5-CF_3	[9]
2	S	S	2-OCH_3	[9]	33	SO_2	SO_2	H	[9]
3	S	S	3-OCH_3	[9]	34	SO_2	SO_2	2-OCH_3	[9]
4	S	S	2-CH_3	[9]	35	SO_2	SO_2	3-OCH_3	[9]
5	S	S	3-CH_3	[9]	36	SO_2	SO_2	4-OCH_3	[9]
6	S	S	4-CH_3	[9]	37	SO_2	SO_2	2-CH_3	[9]
7	S	S	2-Cl	[9]	38	SO_2	SO_2	3-CH_3	[9]
8	S	S	3-Cl	[9]	39	SO_2	SO_2	4-CH_3	[9]
9	S	S	2-Br	[9]	40	SO_2	SO_2	2-Cl	[9]
10	S	S	3-Br	[9]	41	SO_2	SO_2	3-Cl	[9]
11	S	S	3-F	[9]	42	SO_2	SO_2	4-Cl	[9]
12	S	S	3-CN	[9]	43	SO_2	SO_2	2-Br	[9]
13	S	S	4-CN	[9]	44	SO_2	SO_2	3-Br	[9]
14	S	S	3-CF_3	[9]	45	SO_2	SO_2	4-Br	[9]
15	S	S	3-NH_2	[9]	46	SO_2	SO_2	2-F	[9]
16	S	S	3,5-$(CH_3)_2$	[9]	47	SO_2	SO_2	3-F	[9]
17	S	S	3-Cl, 5-CH_3	[9]	48	SO_2	SO_2	2-CN	[9]
18	S	S	3-OCH_3, 5-CH_3	[9]	49	SO_2	SO_2	3-CN	[9]
19	S	S	3-OCH_3, 5-CF_3	[9]	50	SO_2	SO_2	4-CN	[9]
20	SO	SO	2-OCH_3	[9]	51	SO_2	SO_2	3-CF_3	[9]
21	SO	SO	3-OCH_3	[9]	52	SO_2	SO_2	2,5-Cl_2	[9]
22	SO	SO	3-CH_3	[9]	53	SO_2	SO_2	3,5-Cl_2	[9]
23	SO	SO	4-CH_3	[9]	54	SO_2	SO_2	3,5-$(CH_3)_2$	[9]
24	SO	SO	2-Br	[9]	55	SO_2	SO_2	3-Br, 5-CH_3	[9]
25	SO	SO	4-Br	[9]	56	SO_2	SO_2	3-Cl, 5-CH_3	[9]
26	SO	SO	2-CN	[9]	57	SO_2	SO_2	3-OCH_3, 5-CH_3	[9]
27	SO	SO	3-CN	[9]	58	SO_2	SO_2	3-OCH_3, 5-CF_3	[9]
28	SO	SO	3-CF_3	[9]	59	SO_2	SO_2	3-OH, 5-CH_3	[9]
29	SO	SO	3,5-$(CH_3)_2$	[9]	60	SO_2	SO_2	3-OCH_2CH_3, 5-CH_3	[9]
30	SO	SO	2,5-Cl_2	[9]	61	SO_2	SO_2	3-$OCH_2CH_2CH_3$, 5-CH_3	[9]
31	SO	SO	3-Cl, 5-CH_3	[9]					

Computational details

Calculations were performed in gas and water phases by using B3LYP level and 6-311G(d,p) basis set. The Polarized Continuum Model (PCM) method in Gaussian 09 [18] includes a solution that calculates the energy in the solvent by making the electrostatic potential of the reaction field between the solvent and the solute consistent. A more recent version of Integral Equation Formalism PCM (IEFPCM) is used for the water phase calculations.

Quantum chemical parameters related to the reactivity and selectivity of molecules can be estimated from the HOMO and LUMO energies using Koopmans' theorem [45, 46]. These parameters (ionization energy (I), HOMO-LUMO energy difference (ΔE), electronegativity (χ), chemical hardness (η), chemical softness (σ), chemical potential (μ) and global electrophilicity (ω)) were calculated using the following equations (1-9).

The obtained quantum chemical parameters (ionization energy (*I*), HOMO-LUMO energy difference (ΔE), electronegativity (χ), chemical hardness (η), chemical softness (σ), chemical potential (μ) and global electrophilicity (ω)) were calculated with the help of the following equations (1-9) from E_{HOMO} and E_{LUMO} [35, 36, 47-49].

$$I = -E_{HOMO} \quad (1)$$

$$A = -E_{LUMO} \quad (2)$$

$$\Delta E = E_{LUMO} - E_{HOMO} \quad (3)$$

$$\chi = \left(\frac{I+A}{2}\right) \quad (4)$$

Chemical hardness (η) is an indicator of an atom's resistance to charge transfer and is found using eq. 5 below [49]:

$$\eta = \left(\frac{I-A}{2}\right) \quad (5)$$

Chemical softness, an indicator of an atom or group's ability to accept electrons, is calculated using eq. 6 [48].

$$\sigma = \frac{1}{\eta} = -\left(\frac{2}{E_{HOMO}-E_{LUMO}}\right) \quad (6)$$

$$\mu = -\chi = \left(\frac{E_{HOMO}+E_{LUMO}}{2}\right) \quad (7)$$

$$\chi = -\left(\frac{E_{HOMO}+E_{LUMO}}{2}\right) \quad (8)$$

The global electrophilicity index (ω) is a parameter used to compare the electron-donating abilities of molecules [50]. A high value represents a good electrophile, and a low value represents a nucleophile [35, 36, 51]. This value can be estimated using eq. 9.

$$\omega = \frac{\chi^2}{2\eta} \quad (9)$$

Results and discussion

Quantum-chemical Calculations

E_{HOMO}, E_{LUMO}, ΔE, I, η, σ, χ, μ, ω, dipole moment (*DM*), Mulliken atomic charges (*MAC*), molecular volume (*MV*) and the zero-point energies (*ZPE*) values of the investigated 2-amino-6-arylsulfonylbenzonitrile derivatives (1-61) were calculated by using the DFT/B3LYP/6-311G(d,p) method for gas and water phases. All results are displayed in supp. Figs. S1, S2 and Tables 2-4.

Frontier molecular orbital (FMO) theory tells us whether a reaction will occur or not based on the presence or absence of interactions between the HOMO and LUMO frontier orbitals of reacting molecules [52]. Thus, we obtain important information about the activity or stability of a molecule. Some researchers have suggested that the FMO theory is also useful in predicting the interaction center of a molecule [53-55]. It can be easily observed that the HOMO distribution of the studied compounds in the gas phase are mainly around the whole molecule in some compounds, except some small groups such as nitrile, methyl groups, and around of the aryl groups in some compounds such as compounds 37-56 (Fig. S1). The electron-rich regions are believed to be more active. The presence of heteroatoms and sulfur atoms on the tetrazole ring of the molecules studied may lead to stronger adsorption. The presence of the nitrogen atom to give a strong activity of these molecules. The distributions of the LUMO orbitals of the molecules are mainly around the 2-amino benzonitrile and sulfur groups (Fig. S1). LUMO localization at the benzonitrile moiety increased the reactivity of these sites by facilitating electron acceptance. The HOMO and LUMO charge density distribution of studied compounds are depicted in Fig. S1.

Heterocyclic organic compounds containing π-systems and heteroatoms such as O, N, and S are known to be effective corrosion inhibitors [56]. Therefore, the 2-amino-6-arylsulfonylbenzonitrile derivatives we examined can also be used as corrosion inhibitors. Corrosion inhibition occurs through the formation of donor-acceptor surface complexes between the vacant *d*-orbitals of a metal and the π or non-bonding electrons of molecules containing heteroatoms [57]. According to FMO theory, the chemical reactivity of a molecule is a result of the interaction of the HOMO and LUMO orbitals of the reacting atoms and molecules. HOMO orbitals represent a molecule's ability to donate electrons, and LUMO orbitals represent its ability to accept electrons. A high E_{HOMO} value is necessary for reactions with nucleophiles, while a low E_{LUMO} value is necessary for reactions with electrophiles [58]. The chemical hardness (η) and softness (σ) parameters are also widely used to describe the activity and stability of chemical species. Chemical hardness (Eq. 5) is half the energy gap between E_{HOMO} and E_{LUMO}, and if the energy gap is large, it is expressed as hard and if it is small, it is expressed as soft [59]. The smaller ΔE and higher softness values indicate a molecule's greater reactivity, which mechanistically relates to enhanced

electron-donating ability and stronger interaction with the HIV reverse transcriptase active site. These electronic properties directly influence binding affinity and inhibitory efficiency by facilitating charge transfer and stabilizing inhibitor-enzyme complexes.

The high E_{HOMO} values as negative for subset S were as follows: 13 (-6.493 eV), 12 (-6.469 eV) and 14 (-6.365 eV) molecules for the gas phase, and 13 (-6.315 eV), 7 (-6.314 eV) and 9 (-6.312 eV) molecules for the solvent phase. The low E_{HOMO} values as negative were found for 15, 2 and 18 molecules for the gas and solvent phases of subset S. According to the results of E_{HOMO}, it can be assumed that molecule 13 is the most active so a better reactive and molecule 15 is the least active for gas and solvent phases, respectively. The less negative HOMO energy is often interpreted by a stronger adsorption bond and perhaps greater reaction efficiency [55]. According to E_{HOMO} results of set 1, three molecules with the highest reaction efficiency with nucleophiles can be written as: 13 > 12 > 14 for gas phase, and 13 > 7 > 9 for solvent phase. Similarly, molecule 27 for gas phase and molecule 30 for solvent phase of subset SO, and molecule 50 for gas phase and molecule 52 for solvent phase of subset SO_2 that they were found to be the molecules with the most active as nucleophiles. Molecule 20 for subset SO and molecule 34 for subset SO_2 were found to be the most inactive for both gas and solvent phases (Tables 2 and 3).

It is important to note that while the Polarized Continuum Model (PCM) provides valuable insights into solvent effects, continuum models have inherent limitations, such as neglecting specific solute-solvent interactions. These limitations may influence electronic properties such as dipole moment and solvation energy, which in turn could affect biological relevance. Future studies could incorporate explicit solvent molecules or hybrid solvation models to refine these predictions [60].

The E_{LUMO} is an indicator of the molecule's ability to accept electrons. The molecule with a low E_{LUMO} value more easily accepts electrons from electrophiles, and in this case, the adsorption of the molecule on the metal surface will increase and show better reaction. The LUMO results of the molecules examined can be seen from Tables 2 and 3 for both phases. It is known that quantum chemical parameters, energy gap, chemical hardness and chemical softness are related to the chemical properties of molecules [61-65]. Chemical hardness, as proposed by Pearson [56], is defined as the resistance of chemical species to deformation or polarization of the electron cloud. According to the Maximum Hardness Principle (MHP) state: "a chemical system tends to arrange itself so as to achieve maximum hardness, and chemical hardness can be considered as a measurement of stability" [66]. The physical properties of molecules are largely related to ΔE. A high ΔE value indicates the compound's stability and low molecular activity. As the ΔE value increases, it becomes increasingly difficult for molecules to polarize. In this case, it will require more energy to excite the compounds. Molecules with smaller energy gaps will be more easily polarized and will react more readily. [67]. Pearson showed that hard molecules with large ΔE values are more stable than soft molecules with small ΔE values [68, 69]. The smaller ΔE is often related to a stronger adsorption bond and perhaps greater reaction efficiency [55].

Table-2: The calculated quantum chemical parameters for the gas phase.

Molecule	E_{HOMO} (eV)	E_{LUMO} (eV)	ΔE (eV)	I (eV)	η (eV)	σ (eV^{-1})	μ (eV)	χ (eV)	ω (eV)	DM (D)	MAC (e)	MV (cm^3/mol)	ZPE (eV)
1	-6.147	-1.611	4.537	6.147	2.268	0.441	3.879	-3.879	3.317	4.105	-1.799	159.345	-27458.09
2	-5.680	-1.601	4.079	5.680	2.040	0.490	3.640	-3.640	3.248	2.851	-2.340	166.374	-30574.33
3	-5.979	-1.576	4.403	5.979	2.202	0.454	3.778	-3.778	3.241	3.913	-2.240	213.097	-30574.37
4	-6.044	-1.620	4.425	6.044	2.212	0.452	3.832	-3.832	3.319	3.934	-2.062	180.387	-28527.49
5	-6.116	-1.581	4.535	6.116	2.268	0.441	3.849	-3.849	3.266	3.744	-2.041	172.918	-28527.52
6	-6.063	-1.567	4.496	6.063	2.248	0.445	3.815	-3.815	3.237	3.947	-2.025	192.219	-28527.52
7	-6.198	-1.844	4.354	6.198	2.177	0.459	4.021	-4.021	3.714	6.070	-1.842	154.048	-39965.20
8	-6.301	-1.774	4.527	6.301	2.263	0.442	4.037	-4.037	3.601	6.202	-1.915	190.304	-39965.28
9	-6.180	-1.840	4.340	6.180	2.170	0.461	4.010	-4.010	3.706	5.895	-1.793	182.293	-97487.94
10	-6.285	-1.769	4.516	6.285	2.258	0.443	4.027	-4.027	3.591	6.033	-1.837	165.072	-97488.03
11	-6.139	-1.769	4.370	6.139	2.185	0.458	3.954	-3.954	3.578	5.496	-2.086	138.984	-30159.37
12	-6.469	-1.923	4.546	6.469	2.273	0.440	4.196	-4.196	3.873	9.000	-1.895	193.314	-29968.75
13	-6.493	-1.985	4.508	6.493	2.254	0.444	4.239	-4.239	3.987	7.925	-1.848	160.199	-29968.78
14	-6.365	-1.821	4.544	6.365	2.272	0.440	4.093	-4.093	3.686	7.095	-2.552	203.528	-36631.97
15	-5.662	-1.508	4.154	5.662	2.077	0.481	3.585	-3.585	3.093	2.524	-2.167	167.778	-28964.43
16	-6.085	-1.551	4.535	6.085	2.267	0.441	3.818	-3.818	3.214	3.862	-2.293	209.438	-29596.94
17	-6.249	-1.750	4.499	6.249	2.249	0.445	3.999	-3.999	3.555	6.394	-2.200	197.238	-41034.71

18	**-5.925**	**-1.553**	**4.372**	**5.925**	**2.186**	**0.457**	**3.739**	**-3.739**	**3.198**	**4.106**	**-2.501**	**169.211**	**-31643.79**
19	**-6.276**	**-1.737**	**4.539**	**6.276**	**2.269**	**0.441**	**4.007**	**-4.007**	**3.537**	**2.489**	**-3.006**	**219.641**	**-39748.28**
20	**-6.096**	**-1.590**	**4.505**	**6.096**	**2.253**	**0.444**	**3.843**	**-3.843**	**3.278**	**6.480**	**-2.925**	**211.553**	**-32620.10**
21	**-6.270**	**-1.772**	**4.498**	**6.270**	**2.249**	**0.445**	**4.021**	**-4.021**	**3.595**	**6.693**	**-2.810**	**212.176**	**-32620.25**
22	**-6.379**	**-1.822**	**4.557**	**6.379**	**2.278**	**0.439**	**4.100**	**-4.100**	**3.690**	**6.163**	**-2.630**	**177.815**	**-30573.42**
23	**-6.350**	**-1.801**	**4.549**	**6.350**	**2.274**	**0.440**	**4.076**	**-4.076**	**3.652**	**6.538**	**-2.608**	**212.961**	**-30573.41**
24	**-6.401**	**-1.942**	**4.460**	**6.401**	**2.230**	**0.448**	**4.171**	**-4.171**	**3.902**	**7.452**	**-2.343**	**160.427**	**-99533.47**
25	**-6.528**	**-1.976**	**4.552**	**6.528**	**2.276**	**0.439**	**4.252**	**-4.252**	**3.972**	**6.814**	**-2.341**	**177.346**	**-99533.92**
26	**-6.639**	**-2.103**	**4.537**	**6.639**	**2.268**	**0.441**	**4.371**	**-4.371**	**4.211**	**10.267**	**-2.451**	**183.289**	**-32014.27**
27	**-6.649**	**-2.112**	**4.537**	**6.649**	**2.268**	**0.441**	**4.380**	**-4.380**	**4.229**	**10.356**	**-2.468**	**179.238**	**-32014.59**
28	**-6.573**	**-2.027**	**4.546**	**6.573**	**2.273**	**0.440**	**4.300**	**-4.300**	**4.067**	**8.740**	**-3.123**	**204.393**	**-38677.83**
29	**-6.338**	**-1.795**	**4.543**	**6.338**	**2.271**	**0.440**	**4.066**	**-4.066**	**3.640**	**6.394**	**-2.868**	**175.938**	**-31642.85**
30	**-6.597**	**-2.057**	**4.540**	**6.597**	**2.270**	**0.441**	**4.327**	**-4.327**	**4.125**	**6.188**	**-2.461**	**194.082**	**-54517.90**
31	**-6.493**	**-1.937**	**4.557**	**6.493**	**2.278**	**0.439**	**4.215**	**-4.215**	**3.899**	**8.311**	**-2.775**	**195.204**	**-43080.58**
32	**-6.502**	**-1.951**	**4.552**	**6.502**	**2.276**	**0.439**	**4.227**	**-4.227**	**3.925**	**4.693**	**-3.571**	**208.850**	**-41794.15**
33	**-6.581**	**-2.099**	**4.483**	**6.581**	**2.241**	**0.446**	**4.340**	**-4.340**	**4.202**	**6.826**	**-2.829**	**168.882**	**-31550.99**
34	**-6.409**	**-1.964**	**4.445**	**6.409**	**2.222**	**0.450**	**4.187**	**-4.187**	**3.944**	**7.337**	**-3.404**	**185.941**	**-34667.15**
35	**-6.500**	**-2.025**	**4.475**	**6.500**	**2.237**	**0.447**	**4.263**	**-4.263**	**4.060**	**7.236**	**-3.250**	**188.360**	**-34667.26**
36	**-6.490**	**-1.990**	**4.499**	**6.490**	**2.250**	**0.445**	**4.240**	**-4.240**	**3.995**	**7.607**	**-3.282**	**194.031**	**-34667.32**
37	**-6.585**	**-2.054**	**4.531**	**6.585**	**2.265**	**0.441**	**4.320**	**-4.320**	**4.119**	**6.369**	**-3.081**	**198.803**	**-32620.26**
38	**-6.562**	**-2.068**	**4.494**	**6.562**	**2.247**	**0.445**	**4.315**	**-4.315**	**4.143**	**6.637**	**-3.081**	**189.716**	**-32620.44**
39	**-6.539**	**-2.044**	**4.495**	**6.539**	**2.248**	**0.445**	**4.292**	**-4.292**	**4.098**	**6.861**	**-3.062**	**203.634**	**-32620.44**
40	**-6.634**	**-2.120**	**4.514**	**6.634**	**2.257**	**0.443**	**4.377**	**-4.377**	**4.244**	**7.590**	**-2.778**	**206.232**	**-44057.76**
41	**-6.672**	**-2.238**	**4.434**	**6.672**	**2.217**	**0.451**	**4.455**	**-4.455**	**4.476**	**7.623**	**-2.942**	**225.269**	**-44058.14**
42	**-6.687**	**-2.239**	**4.448**	**6.687**	**2.224**	**0.450**	**4.463**	**-4.463**	**4.479**	**6.848**	**-2.842**	**161.723**	**-44058.18**
43	**-6.644**	**-2.117**	**4.526**	**6.644**	**2.263**	**0.442**	**4.380**	**-4.380**	**4.239**	**7.491**	**-2.798**	**220.069**	**-101580.49**
44	**-6.667**	**-2.229**	**4.438**	**6.667**	**2.219**	**0.451**	**4.448**	**-4.448**	**4.457**	**7.506**	**-2.856**	**220.403**	**-101580.88**
45	**-6.680**	**-2.230**	**4.450**	**6.680**	**2.225**	**0.449**	**4.455**	**-4.455**	**4.459**	**6.822**	**-2.775**	**158.391**	**-101580.92**
46	**-6.596**	**-2.111**	**4.485**	**6.596**	**2.243**	**0.446**	**4.353**	**-4.353**	**4.225**	**7.340**	**-3.060**	**169.127**	**-34252.04**
47	**-6.660**	**-2.217**	**4.443**	**6.660**	**2.221**	**0.450**	**4.438**	**-4.438**	**4.434**	**7.453**	**-3.008**	**187.406**	**-34252.28**
48	**-6.751**	**-2.336**	**4.415**	**6.751**	**2.208**	**0.453**	**4.543**	**-4.543**	**4.675**	**9.813**	**-2.893**	**205.831**	**-34061.25**
49	**-6.788**	**-2.396**	**4.393**	**6.788**	**2.196**	**0.455**	**4.592**	**-4.592**	**4.800**	**9.303**	**-2.912**	**195.740**	**-34061.57**
50	**-6.820**	**-2.589**	**4.231**	**6.820**	**2.116**	**0.473**	**4.704**	**-4.704**	**5.230**	**7.839**	**-2.839**	**251.207**	**-34061.59**
51	**-6.707**	**-2.193**	**4.514**	**6.707**	**2.257**	**0.443**	**4.450**	**-4.450**	**4.387**	**8.757**	**-3.498**	**199.699**	**-40724.37**
52	**-6.721**	**-2.241**	**4.480**	**6.721**	**2.240**	**0.446**	**4.481**	**-4.481**	**4.482**	**6.559**	**-2.910**	**218.233**	**-56564.90**
53	**-6.767**	**-2.377**	**4.390**	**6.767**	**2.195**	**0.456**	**4.572**	**-4.572**	**4.761**	**7.094**	**-3.128**	**212.277**	**-56565.26**
54	**-6.536**	**-2.032**	**4.504**	**6.536**	**2.252**	**0.444**	**4.284**	**-4.284**	**4.074**	**6.782**	**-3.332**	**207.521**	**-33689.87**
55	**-6.635**	**-2.189**	**4.446**	**6.635**	**2.223**	**0.450**	**4.412**	**-4.412**	**4.377**	**7.715**	**-3.139**	**245.575**	**-102650.32**
56	**-6.642**	**-2.198**	**4.444**	**6.642**	**2.222**	**0.450**	**4.420**	**-4.420**	**4.396**	**7.838**	**-3.232**	**229.079**	**-45127.58**
57	**-6.454**	**-1.993**	**4.461**	**6.454**	**2.230**	**0.448**	**4.223**	**-4.223**	**3.999**	**7.398**	**-3.513**	**194.664**	**-35736.69**
58	**-6.657**	**-2.225**	**4.432**	**6.657**	**2.216**	**0.451**	**4.441**	**-4.441**	**4.450**	**6.131**	**-4.006**	**234.512**	**-43841.12**
59	**-6.504**	**-2.028**	**4.476**	**6.504**	**2.238**	**0.447**	**4.266**	**-4.266**	**4.066**	**7.654**	**-3.370**	**177.601**	**-34667.76**
60	**-6.430**	**-1.988**	**4.442**	**6.430**	**2.221**	**0.450**	**4.209**	**-4.209**	**3.988**	**7.366**	**-3.731**	**260.892**	**-36806.15**
61	**-6.428**	**-1.991**	**4.437**	**6.428**	**2.218**	**0.451**	**4.210**	**-4.210**	**3.994**	**7.314**	**-3.962**	**224.681**	**-37875.46**

E_{HOMO}: The energy of the highest occupied molecular orbital, E_{LUMO}: The energy of the lowest unoccupied molecular orbital, ΔE: HOMO-LUMO energy gap, *I*: Ionization potential, *DM*: Dipole moment, *MAC*: Mulliken atomic charges, η: Chemical hardness, σ: Chemical softness, χ: Electronegativity, μ: Chemical potential, ω: Global electrophilicity, *MV*: Molecular volume, *ZPE*: The zero-point energies.

Table-3: The calculated quantum chemical parameters for the water phase.

Molecule	E_{HOMO} **(eV)**	E_{LUMO} **(eV)**	ΔE **(eV)**	***I*** **(eV)**	η **(eV)**	σ **(eV^{-1})**	μ **(eV)**	χ **(eV)**	ω **(eV)**	***DM*** **(D)**	***MAC*** **(e)**	***MV*** **(cm^3/mol)**	***ZPE*** **(eV)**
1	**-6.202**	**-1.746**	**4.456**	**6.202**	**2.228**	**0.449**	**3.974**	**-3.974**	**3.543**	**6.148**	**-1.959**	**176.685**	**-27458.46**
2	**-5.995**	**-1.760**	**4.235**	**5.995**	**2.117**	**0.472**	**3.877**	**-3.877**	**3.550**	**4.768**	**-2.498**	**202.808**	**-30574.78**
3	**-6.189**	**-1.745**	**4.444**	**6.189**	**2.222**	**0.450**	**3.967**	**-3.967**	**3.542**	**6.086**	**-2.412**	**186.364**	**-30574.79**
4	**-6.176**	**-1.754**	**4.422**	**6.176**	**2.211**	**0.452**	**3.965**	**-3.965**	**3.555**	**5.912**	**-2.220**	**139.105**	**-28527.85**
5	**-6.184**	**-1.737**	**4.447**	**6.184**	**2.224**	**0.450**	**3.960**	**-3.960**	**3.527**	**5.618**	**-2.186**	**194.152**	**-28527.88**
6	**-6.163**	**-1.721**	**4.442**	**6.163**	**2.221**	**0.450**	**3.942**	**-3.942**	**3.498**	**5.909**	**-2.173**	**187.453**	**-28527.89**
7	**-6.314**	**-1.844**	**4.471**	**6.314**	**2.235**	**0.447**	**4.079**	**-4.079**	**3.721**	**8.567**	**-1.968**	**147.371**	**-39965.59**
8	**-6.236**	**-1.780**	**4.456**	**6.236**	**2.228**	**0.449**	**4.008**	**-4.008**	**3.605**	**8.901**	**-2.017**	**177.848**	**-39965.66**
9	**-6.312**	**-1.851**	**4.461**	**6.312**	**2.230**	**0.448**	**4.082**	**-4.082**	**3.735**	**8.362**	**-1.926**	**217.623**	**-97488.33**

10	**-6.255**	**-1.799**	**4.456**	**6.255**	**2.228**	**0.449**	**4.027**	**-4.027**	**3.639**	**8.671**	**-1.947**	**208.640**	**-97488.41**
11	**-6.279**	**-1.811**	**4.468**	**6.279**	**2.234**	**0.448**	**4.045**	**-4.045**	**3.662**	**7.976**	**-2.206**	**173.998**	**-30159.76**
12	**-6.283**	**-1.852**	**4.431**	**6.283**	**2.216**	**0.451**	**4.067**	**-4.067**	**3.733**	**12.266**	**-2.039**	**214.433**	**-29969.23**
13	**-6.315**	**-1.859**	**4.457**	**6.315**	**2.228**	**0.449**	**4.087**	**-4.087**	**3.748**	**10.687**	**-2.024**	**157.750**	**-29969.27**
14	**-6.264**	**-1.799**	**4.465**	**6.264**	**2.232**	**0.448**	**4.031**	**-4.031**	**3.640**	**9.810**	**-2.648**	**209.063**	**-36632.36**
15	**-5.821**	**-1.725**	**4.095**	**5.821**	**2.048**	**0.488**	**3.773**	**-3.773**	**3.476**	**4.057**	**-2.360**	**181.394**	**-28964.91**
16	**-6.157**	**-1.722**	**4.435**	**6.157**	**2.217**	**0.451**	**3.940**	**-3.940**	**3.500**	**5.806**	**-2.417**	**147.868**	**-29597.31**
17	**-6.244**	**-1.786**	**4.458**	**6.244**	**2.229**	**0.449**	**4.015**	**-4.015**	**3.616**	**9.185**	**-2.302**	**173.909**	**-41035.10**
18	**-6.155**	**-1.737**	**4.417**	**6.155**	**2.209**	**0.453**	**3.946**	**-3.946**	**3.525**	**6.471**	**-2.652**	**213.266**	**-31644.22**
19	**-6.265**	**-1.797**	**4.468**	**6.265**	**2.234**	**0.448**	**4.031**	**-4.031**	**3.637**	**3.808**	**-3.137**	**218.112**	**-39748.70**
20	**-6.174**	**-1.745**	**4.429**	**6.174**	**2.214**	**0.452**	**3.960**	**-3.960**	**3.540**	**9.989**	**-3.114**	**221.120**	**-32620.73**
21	**-6.346**	**-1.921**	**4.425**	**6.346**	**2.213**	**0.452**	**4.133**	**-4.133**	**3.861**	**9.844**	**-3.002**	**210.393**	**-32620.86**
22	**-6.340**	**-1.914**	**4.426**	**6.340**	**2.213**	**0.452**	**4.127**	**-4.127**	**3.848**	**9.062**	**-2.780**	**197.156**	**-30573.96**
23	**-6.338**	**-1.908**	**4.430**	**6.338**	**2.215**	**0.451**	**4.123**	**-4.123**	**3.837**	**9.606**	**-2.771**	**181.678**	**-30573.96**
24	**-6.343**	**-2.013**	**4.330**	**6.343**	**2.165**	**0.462**	**4.178**	**-4.178**	**4.031**	**8.010**	**-2.481**	**170.180**	**-99534.33**
25	**-6.361**	**-1.960**	**4.401**	**6.361**	**2.201**	**0.454**	**4.161**	**-4.161**	**3.933**	**9.791**	**-2.486**	**182.310**	**-99534.46**
26	**-6.412**	**-2.045**	**4.366**	**6.412**	**2.183**	**0.458**	**4.229**	**-4.229**	**4.095**	**14.869**	**-2.629**	**202.338**	**-32015.04**
27	**-6.386**	**-1.999**	**4.387**	**6.386**	**2.194**	**0.456**	**4.192**	**-4.192**	**4.007**	**14.414**	**-2.650**	**206.123**	**-32015.27**
28	**-6.377**	**-1.983**	**4.394**	**6.377**	**2.197**	**0.455**	**4.180**	**-4.180**	**3.977**	**12.320**	**-3.265**	**189.851**	**-38678.41**
29	**-6.336**	**-1.911**	**4.426**	**6.336**	**2.213**	**0.452**	**4.123**	**-4.123**	**3.842**	**9.457**	**-3.010**	**202.257**	**-31643.39**
30	**-6.439**	**-2.144**	**4.295**	**6.439**	**2.148**	**0.466**	**4.292**	**-4.292**	**4.289**	**9.832**	**-2.634**	**223.669**	**-31551.56**
31	**-6.365**	**-1.964**	**4.401**	**6.365**	**2.201**	**0.454**	**4.164**	**-4.164**	**3.940**	**11.998**	**-2.928**	**201.538**	**-43081.15**
32	**-6.374**	**-1.976**	**4.398**	**6.374**	**2.199**	**0.455**	**4.175**	**-4.175**	**3.964**	**7.124**	**-3.721**	**263.991**	**-41794.74**
33	**-6.439**	**-2.144**	**4.295**	**6.439**	**2.148**	**0.466**	**4.292**	**-4.292**	**4.289**	**9.832**	**-2.969**	**223.669**	**-31551.56**
34	**-6.349**	**-2.069**	**4.280**	**6.349**	**2.140**	**0.467**	**4.209**	**-4.209**	**4.139**	**11.278**	**-3.567**	**202.026**	**-34667.79**
35	**-6.430**	**-2.138**	**4.292**	**6.430**	**2.146**	**0.466**	**4.284**	**-4.284**	**4.276**	**10.465**	**-3.425**	**160.889**	**-34667.89**
36	**-6.410**	**-2.090**	**4.320**	**6.410**	**2.160**	**0.463**	**4.250**	**-4.250**	**4.181**	**10.998**	**-3.443**	**231.660**	**-34667.95**
37	**-6.440**	**-2.086**	**4.354**	**6.440**	**2.177**	**0.459**	**4.263**	**-4.263**	**4.173**	**9.234**	**-3.232**	**182.892**	**-32620.81**
38	**-6.436**	**-2.128**	**4.307**	**6.436**	**2.154**	**0.464**	**4.282**	**-4.282**	**4.257**	**9.558**	**-3.212**	**195.420**	**-32621.00**
39	**-6.424**	**-2.115**	**4.309**	**6.424**	**2.154**	**0.464**	**4.270**	**-4.270**	**4.231**	**10.017**	**-3.204**	**174.304**	**-32621.02**
40	**-6.499**	**-2.194**	**4.305**	**6.499**	**2.153**	**0.465**	**4.347**	**-4.347**	**4.389**	**11.871**	**-2.953**	**168.550**	**-44058.42**
41	**-6.462**	**-2.220**	**4.243**	**6.462**	**2.121**	**0.471**	**4.341**	**-4.341**	**4.442**	**10.867**	**-3.071**	**222.892**	**-44058.70**
42	**-6.454**	**-2.204**	**4.250**	**6.454**	**2.125**	**0.471**	**4.329**	**-4.329**	**4.410**	**9.704**	**-2.963**	**225.609**	**-44058.72**
43	**-6.494**	**-2.188**	**4.306**	**6.494**	**2.153**	**0.464**	**4.341**	**-4.341**	**4.375**	**11.619**	**-2.931**	**192.840**	**-101581.15**
44	**-6.460**	**-2.218**	**4.241**	**6.460**	**2.121**	**0.472**	**4.339**	**-4.339**	**4.439**	**10.803**	**-2.980**	**190.859**	**-101581.45**
45	**-6.451**	**-2.200**	**4.251**	**6.451**	**2.126**	**0.470**	**4.326**	**-4.326**	**4.401**	**9.690**	**-2.892**	**174.348**	**-101581.47**
46	**-6.457**	**-2.160**	**4.297**	**6.457**	**2.148**	**0.465**	**4.309**	**-4.309**	**4.321**	**10.831**	**-3.204**	**171.029**	**-34252.66**
47	**-6.457**	**-2.211**	**4.246**	**6.457**	**2.123**	**0.471**	**4.334**	**-4.334**	**4.424**	**10.647**	**-3.130**	**194.251**	**-34252.85**
48	**-6.496**	**-2.371**	**4.126**	**6.496**	**2.063**	**0.485**	**4.434**	**-4.434**	**4.764**	**14.407**	**-3.059**	**215.645**	**-34062.02**
49	**-6.482**	**-2.288**	**4.194**	**6.482**	**2.097**	**0.477**	**4.385**	**-4.385**	**4.585**	**12.891**	**-3.078**	**195.449**	**-34062.24**
50	**-6.475**	**-2.523**	**3.952**	**6.475**	**1.976**	**0.506**	**4.499**	**-4.499**	**5.122**	**10.567**	**-2.988**	**166.667**	**-34062.24**
51	**-6.490**	**-2.180**	**4.310**	**6.490**	**2.155**	**0.464**	**4.335**	**-4.335**	**4.361**	**12.940**	**-3.662**	**224.349**	**-40725.04**
52	**-6.517**	**-2.241**	**4.276**	**6.517**	**2.138**	**0.468**	**4.379**	**-4.379**	**4.484**	**9.873**	**-3.057**	**221.600**	**-56565.52**
53	**-6.480**	**-2.300**	**4.180**	**6.480**	**2.090**	**0.478**	**4.390**	**-4.390**	**4.611**	**9.941**	**-3.254**	**224.142**	**-56565.79**
54	**-6.427**	**-2.114**	**4.313**	**6.427**	**2.156**	**0.464**	**4.270**	**-4.270**	**4.229**	**9.902**	**-3.456**	**209.375**	**-33690.44**
55	**-6.455**	**-2.201**	**4.253**	**6.455**	**2.127**	**0.470**	**4.328**	**-4.328**	**4.404**	**11.162**	**-3.275**	**219.178**	**-102650.90**
56	**-6.455**	**-2.206**	**4.249**	**6.455**	**2.125**	**0.471**	**4.330**	**-4.330**	**4.413**	**11.292**	**-3.371**	**205.519**	**-45128.15**
57	**-6.424**	**-2.126**	**4.298**	**6.424**	**2.149**	**0.465**	**4.275**	**-4.275**	**4.252**	**10.786**	**-3.678**	**167.067**	**-35737.33**
58	**-6.462**	**-2.237**	**4.225**	**6.462**	**2.113**	**0.473**	**4.349**	**-4.349**	**4.477**	**8.872**	**-4.140**	**221.526**	**-43841.74**
59	**-6.424**	**-2.135**	**4.289**	**6.424**	**2.145**	**0.466**	**4.280**	**-4.280**	**-4.271**	**11.073**	**-3.532**	**185.290**	**-34668.46**
60	**-6.423**	**-2.126**	**4.297**	**6.423**	**2.148**	**0.465**	**4.274**	**-4.274**	**4.252**	**10.778**	**-3.899**	**213.718**	**-36806.79**
61	**-6.424**	**-2.126**	**4.298**	**6.424**	**2.149**	**0.465**	**4.275**	**-4.275**	**4.252**	**10.704**	**-4.128**	**252.177**	**-37876.09**

E_{HOMO}: The energy of the highest occupied molecular orbital, E_{LUMO}: The energy of the lowest unoccupied molecular orbital, ΔE: HOMO-LUMO energy gap, *I*: Ionisation potential, *DM*: Dipole moment, *MAC*: Mulliken atomic charges, η: Chemical hardness, σ: Chemical softness, χ: Electronegativity, μ: Chemical potential, ω: Global electrophilicity, *MV*: Molecular volume, *ZPE*: The zero-point energies.

According to ΔE values, the three molecules with the highest reaction efficiency ranking for the gas phase are 2 (4.079 eV) > 15 (4.154 eV) > 9 (4.340 eV), and 15 (4.095 eV) > 2 (4.235 eV) > 18 (4.417 eV) for the solvent phase of subset S. Generally, ΔE values in the gas phase are lower than the water phase for subset S. Therefore, the water phase is expected to be a higher reaction stable for subset S than the gas phase. It can be seen, from Table 2, that the ΔE values are very close to each other for the gas phase. According to these results, molecules 2, 15, 9 for the gas phase and molecules 15, 2, 18 for the solvent phase are expected to act as higher reaction efficiency than other molecules due to their lower ΔE values (Tables 2 and 3). Similarly, molecules 24, 21, 20 for the gas phase and 30, 24, 26 for the solvent phase of subset SO, and 50, 53, 49 for the gas phase and 50, 48, 53 for the solvent phase of subset SO_2 are expected to act as higher reaction efficiency (Tables 2 and 3). To summarize, compounds 2, 24 and 50 for gas phase, and 15, 30 and 50 for water phase showed the smallest ΔE values (4.079–4.231 eV for gas phase and 4.095-4.295 eV for water phase) indicating high reactivity.

A molecule's high ionization potential (I) indicates chemical inertness and high stability, while a low value indicates a species' high activity [64]. According to the I value, the three molecules with the highest activation order can be written as: 15 > 2 > 18 for gas and water phases for subset S. I values in the gas phase are lower than the solvent phase for 15, 2 and 18 molecules. Molecule 15 is more active than other molecules for the gas and solvent phases, owing to its lowest ionization potential values. 13 is the most inactive molecule for the gas and solvent phases of subset S, while 20, 21, 29 and 20, 29, 23 are the most active molecules respectively for the gas and solvent phases for subset SO, and 34, 61, 60 for the gas phase and 34, 36, 60 for the solvent phase of subset SO_2 (Tables 2 and 3).

The chemical hardness (η) and softness (σ) parameters are also widely used to describe the activity and stability of chemical species. Chemical hardness (Eq. 5) is half the energy gap between E_{HOMO} and E_{LUMO}, and if the energy gap is large, it is expressed as hard and if it is small, it is expressed as soft [67]. On the basis of the calculated chemical hardness and softness values in Tables 2 and 3, the order of activity for subset S molecules under investigation is: 2 > 15 > 9 for the gas phase and 15 > 2 > 18 for the solvent phase. The results of subsets 2 and 3 can be seen in Tables 2 and 3. Active molecules have a greater softness value than inactive ones. Chemical softness (Eq. 6) is an indicator of polarization. Soft molecules can more easily donate electrons to an opposite electron-accepting molecule or surface [19]. Softness values for subsets S, SO and SO_2 can be seen in Tables 2 and 3. Molecule 2 for gas phase and molecule 15 for the solvent phase are expected to have higher activity than other molecules for subset S.

Chemical hardness, electronegativity and chemical potential are very useful parameters in predicting the chemical properties of molecules [70]. Electronegativity is also an indicator of a molecule's tendency to attract electrons, that is, its electron density. Electronegativity measures the ability of chemical species to attract electrons and is a useful quantity in estimating the activity of molecules [19]. In general, a molecule with lower electronegativity tends to donate electrons more easily and therefore exhibits higher activity than a molecule with higher electronegativity [71].

Compounds with higher activity have a higher softness value. Chemical softness is a measure of polarizability, and soft molecules are more likely to donate electrons to an electron-accepting molecule or surface [19]. According to the softness values of subsets S, SO and SO_2 in Tables 2 and 3, the activity ranking is similar as the hardness for all subsets. Molecule 2 for gas phase and molecule 15 for the solvent phase are expected to have higher activity than other molecules for subset S.

The electronegativity values were determined as: 15 (-3.585 eV), 2 (-3.640 eV), 18 (-3.739 eV) for the gas phase and 15 (-3.773 eV), 2 (-3.877 eV), 16 (-3.940 eV) for the solvent phase of subset S, and 20 (-3.843 eV), 21 (-4.021 eV), 29 (-4.066 eV) for the gas phase and 20 (-3.960 eV), 29 (-4.123 eV), 23 (-4.123 eV) for the solvent phase of subset SO, and 34 (-4.187 eV), 60 (-4.209 eV), 61 (-4.210 eV) for the gas phase and 34 (-4.209 eV), 36 (-4.250 eV), 37 (-4.263 eV) for the solvent phase of subset SO_2. The lower electronegativity values of compound 15 suggests higher activity, as compared to the other molecules for both phases of subset S, compounds 20 and 34 respectively for both phases of subsets SO and SO_2 (see Tables 2 and 3).

Dipole moment (DM) can be used as an indicator of the activity of chemical species. While some authors have reported no clear relationship between DM and reaction efficiency [62, 63], others suggest that reaction efficiency increases with increasing dipole moment [72-74]. Some studies also emphasize that increasing DM facilitates the electron transport process [73, 74]. According to the DM

results, the reaction efficiency can be summarized as follows for the three molecules with the highest efficiency: 12 > 13 > 14 for the gas and solvent phases of subset S, 27 > 26 > 28 for the gas phase and 26 > 27 > 28 for the solvent phase of subset SO, and 48 > 49 > 51 for the gas phase and 48 > 51 > 49 for the solvent phase of subset SO_2.

Another parameter to consider is the Mulliken atomic charges (*MAC*), which can give valuable information about the reactive behaviour of the molecules under study, by summing all the negative loads in a molecule [72]. A high MAC value means that the reaction activity of the molecule is increased [28]. According to the obtained dipole moment results, 12, 26 and 48 correspond to the best active molecules for the gas and solvent phases of subsets S, SO and SO_2, respectively (see Tables 2 and 3).

The molecule with higher the zero-point energies (*ZPE*) is the hardest electron-donating and the most stable [75]. According to *ZPE* results, compound 10 represents the best reactive in the gas phase and compound 9 in the water phase of subset S. The results for subsets SO and SO_2 can be seen from Table 2 for the gas phase and Table 3 for the solvent phase.

Molecular volume (MV) has been found to indicate the potential inhibitor coverage on a metal surface. A molecule with a larger MV can provide better protection on the metal surface because it has a larger surface area [76]. The calculated MV values for the gas and solvent phases of the investigated molecules are given in Tables 2 and 3.

Quantum chemical studies can also provide useful information to better understand the structural conformation and molecular behaviour of molecules. The electrostatic potential (ESP) distributions of a compound can be studied more precisely with the DFT approach [67]. ESP can describe the electrostatic interaction between an atom and a molecule. ESP provides information about the nucleophilic and electrophilic nature of molecules. ESP is an important tool for investigating and studying the reactivity of molecules. ESP maps for the series of molecules studied are shown in Fig. S2.

Examining Fig. S2, different colors are visible in the ESP maps of the molecules. The bluish regions in these maps represent the positive region where the nucleophilic reaction occurs, and the reddish regions represent the negative region where the electrophilic reaction occurs. When Fig. S2 is examined, it is seen that the electron density around the nitrogen and oxygen atoms with negative electrostatic potential values of the examined molecules increases. Particularly, most of the electrophilic reactions take place in the red regions where the electron density of nitrogen and oxygen atoms is high. These regions featuring maximum electronegativity can be observed in Fig. S2. This result shows that nitrogen and oxygen atoms in molecules will participate more easily in electrophilic reactions.

In theoretical studies, electronic charge analyses of atoms in molecules provide important information. The binding capacity of a molecule is related to the electronic charge of the heteroatoms within the molecule. It has been observed that as the negative charge on the heteroatom increases, binding becomes easier [77]. In this study, Mulliken population analysis [78] was used to calculate the atomic charges of molecules. It can be seen that nitrogen and oxygen atoms with electron-rich regions have higher Mulliken atomic charges (Tables 2 and 3).

Correlations

We computed correlations between quantum descriptor variables and pIC_{50} values (Table S1) for the whole data set (61 compounds). The results are summarized in Table S2. All correlation values in bold are statistically significant at a 0.05 significance level. The values below the diagonal of the Table S2 and the other tables are symmetric so we left it blank. Then, we calculated correlations between quantum descriptor variables and pIC_{50} for the data subset S (Table S3). Afterward, we calculated correlations between quantum descriptor variables and pIC_{50} for the data subset SO (Table S4), and finally, we calculated correlations between quantum descriptor variables and pIC_{50} for the data subset SO_2 (Table S5). By doing so, linearity or non-linearity relations between attributes and pIC_{50} values were determined to help us select relatively the best models using significant attributes.

Statistical analysis for gas phase

To verify this segmentation statistically, we conducted a statistical analysis called Linear Support Vector Machine (LSVM) using Mat Lab 7.9 running 5-fold cross-validation with the dependent variable pIC_{50} and 13 descriptor variables, namely, E_{HOMO}, E_{LUMO}, ΔE, *I*, *DM*, *MAC*, η, σ, μ, χ, ω, *MV* and *ZPE*.

The prediction accuracy of the LSVM is 91.8%, which is statistically quite high. Fig. 1 exhibits the output of the analysis. Each colour represents one subset. In Fig. 1, each subset is represented by different colours such as blue, red, and yellow due to the clustering algorithm called Linear Support Vector Machine. The clustering accuracy is statistically very high, which is almost 92 percent. However, some of the compounds represented by the red colour have overlapping properties with other subsets such as blue and yellow. Even though the axes of Fig. 1 are called *DM* and *I*, this is one of the generic representations since the same graphs were generated using other pairs of attributes by Mat Lab 7.9. Hence, we decided to run a separate statistical analysis for each of the three subsets. For the first subset (S) consisting of **1-19** compounds, we constructed a model between the dependent variables called pIC_{50} and 13 independent variables called descriptors, namely, E_{HOMO}, E_{LUMO}, ΔE, *I, DM, MAC,* η, σ, μ, χ, ω, *MV* and *ZPE*. Subset S is split into three heterogeneous sub-groups. While the first sub-group is composed of compounds 8, 9, 10, 11, 13, 14 and 19, the second sub-group consists of compounds 1, 3, 4, 5, 15, 16 and 18. The last sub-group contains the rest i.e., compounds 2, 6, 7, 12**,** and **17**. We defined a new variable called *M* by:

$$M = \frac{\Delta E}{I}$$

For the first sub-group, the constructed model using compounds 8, 9, 10, 11, 13, 14 and 19, the pIC_{50} was determined using the equation below:

$$\sqrt{pIC_{50}} = -7.88 + 13.015 * M$$

where $M = \frac{\Delta E}{I}$

The determination of the coefficient, R^2 = 0.95, is very high. In addition, the whole model is statistically significant since 0.00 < 0.05 and 0.00 < 0.05 are significant values for constant and variable *M* obtained using SPSS 24.0 version, respectively. For the second sub-group, the constructed model using compounds 1, 3, 4, 5, 15, 16 and 18 is:

$$\sqrt{pIC_{50}} = -25.96 + 37.19 * M$$

where $M = \frac{\Delta E}{I}$

The determination of the coefficient, R^2 = 0.66, is high. In addition, the whole model is statistically significant since 0.032 < 0.05 and 0.026 < 0.05 are significant values for constant and *M* variable calculated using SPSS 24.0 version, respectively.

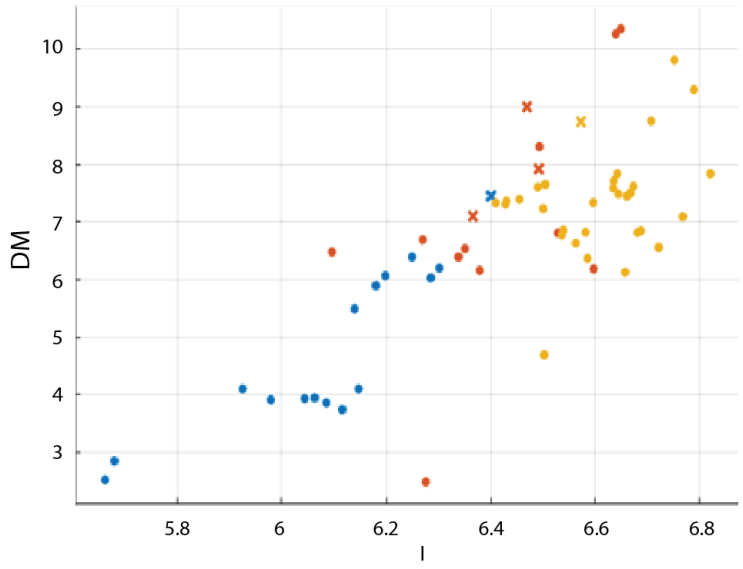

Fig. 1: The output of Mat Lab 7.9 running prediction method called Linear Support Vector Machine between dipole moment (*DM*) and ionization potential (*I*).

For the third sub-group, the constructed model using compounds 2, 6, 7, 12 and 17 can be described by:

$$\sqrt{\mathrm{pIC_{50}}} = 12.29 - 15.082 * M$$

where $M = \frac{\Delta E}{I}$

The determination of the coefficient, R^2 = 0.70, is high. In addition, the whole model is statistically significant since 0.00 < 0.031 and 0.044 < 0.005 are significant values for constant and *M* variable obtained using SPSS 24.0 version, respectively. Then, we examined the second subset (SO) consisting of compounds 20-32. Subset SO has 2 heterogeneous sub-groups. While the first one is composed of compounds 21, 22, 23, 24, 25, 28, 30 and 32, the second one consists of compounds 20, 26, 27, 29 and 31. We defined a new variable called N by:

$$N = \frac{I + DM}{EN * Electrophily}$$

We constructed two different models. The first sub-group, consisting of compounds 21, 22, 23, 24, 25, 28, 30 and 32, is represented by a model as follows:

$$\sqrt{\mathrm{pIC_{50}}} = 2.688 - 1.702 * N$$

where $N = \frac{I+DM}{EN*Electrophily}$

Here again, R^2 = 0.70 thus, referring to a statistically significant model. On the other hand, for the second sub-group consisting of compounds 20, 26, 27, 29 and 31, it is described by the following equation:

$$\sqrt{\mathrm{pIC_{50}}} = -203.98 + 350.88 * N - 150.79 * N^3$$

where $N = \frac{I+DM}{EN*Electrophily}$

With R^2 = 0.89, the whole model is statistically significant since 0.02 < 0.05, 0.031 < 0.05 and 0.022 < 0.05 are significant values for constant, the *N* and N^3 variables determined using SPSS 24.0 version, respectively. The total number of compounds under investigation is 61 and the compounds numbered between 33 and 61 presented in Table 1 are related to the third subset denoted by SO_2. All are utilized to construct models between pIC_{50} and descriptor variables. The first sub-group of those molecules whose numbers are called 33, 34, 35, 37, 40, 42, 43, 45, 46, 47, 48, 49, 58, 59, 60 and 61 generates a model, as follows:

$$\mathrm{pIC_{50}} = -2.715 - 1.785 * MAC$$

The value of R^2 = 0.86 is very high. The whole model is found to be statistically significant with 0.00 < 0.05, 0.00 < 0.05 significant values for constant and the *MAC* variable. On the other hand, the second sub-group of those molecules (36, 39, 51, 53) generates another model, as follows:

$$\sqrt{\mathrm{pIC_{50}}} = -8.341 + 15.917 * M$$

where $M = \frac{\Delta E}{I}$

The R^2 = 0.90 is very high. The whole model is found to be statistically significant with 0.007 < 0.05, 0.004 < 0.05 significant values for constant and the variable *M*. The third sub-group of those molecules corresponding to 38, 41, 44, 50, 52 and 54 generates another model, as follows:

$$\sqrt{\mathrm{pIC_{50}}} = 12.860 - 16.707 * M$$

where $M = \frac{\Delta E}{I}$

The determination of coefficient, R^2 = 0.95, is very high. 0.006 < 0.05, 0.007 < 0.05 are obtained for constant and the *M* variable that denotes a statistically significant model.

Statistical analysis for water phase

Before starting data analysis, the original data set of the 61 compounds is split into 3, as previously. 1–19: Subset S, 20–32: Subset SO, and 33–61: Subset SO_2. To verify this segmentation statistically, we performed a statistical analysis called Linear Discriminant Analysis (LDA) using Mat Lab 7.9 version running 5-fold cross-validation, employing dependent variable called pIC_{50} and 13 descriptor variables, namely, E_{HOMO}, E_{LUMO}, ΔE, *I, DM, MAC,* η, σ, μ, χ, ω, *MV* and *ZPE*. The prediction accuracy of the LDA is 91.8%, which is statistically very high. Fig. 2 depicts the output of the analysis.

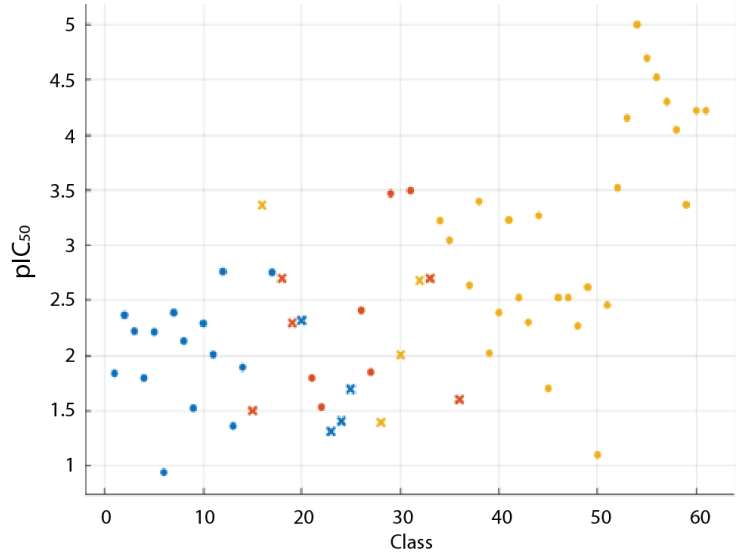

Fig. 2: The output of Mat Lab 7.9 running Linear Discriminant Analysis Method between pIC_{50} and class.

In Fig. 2, each colour represents a different subset such as blue, red, and yellow. The molecules represented by the red have overlapping properties with molecules represented by yellow and blue. Fig. 2 is a generic representation for all attributes since we can generate very similar graphs using other pairs of attributes. Therefore, we decided to run a separate statistical analysis for each of the three subsets. For the first subset (S) consisting of 19 compounds, we built a model between the dependent variable called pIC_{50} and 13 independent variables called descriptors, namely, E_{HOMO}, E_{LUMO}, ΔE, *I, DM, MAC,* η, σ, μ, χ, ω, *MV* and *ZPE*. Subset S is split into four heterogeneous sub-groups. The sub-group 1 comprises compounds 2, 3, 4, 5, 8, 10, 11, and 19, the sub-group 2 consists of compounds 6, 12, 14, 15, and 18, the Sub-group 3 is composed of compounds 1, 9 and 13, the sub-group 4 consists of compounds 7, 16 and 17.

For the sub-groups 1, 2, 3, and 4, we defined a new variable called *K*, as follows:

$$K = \frac{\sqrt{MV}}{I}$$

Then, a linear regression method is conducted to construct a model between pIC_{50} and *K*. For the sub-group S (compounds 2, 3, 4, 5, 8, 10, 11, 19), the constructed model is determined as follows:

$$pIC_{50} = -0.422 + 1.173 * K$$

where the determination of coefficient, $R^2 = 0.96$, is very high and the p-value is $0.00 < 0.05$. For sub-group SO (compounds 6, 12, 14, 15, 18), the constructed model is represented by

$$pIC_{50} = -26.775 + 12.434 * K$$

The constructed model generates $R^2 = 0.77$, which is high and the p-value is $0.045 < 0.05$. The sub-group SO_2 (compounds 1, 9, 13) generates a model defined by

$$pIC_{50} = -13.56 + 59.17 * K - 62.7 * K^2$$

For this model, $R^2 = 0.98$ is very high and the p-value is $0.01 < 0.05$. The sub-group 4 (compounds 7, 16, 17) leads to a model defined by

$$pIC_{50} = -110.8 + 448.4 * K - 450.1 * K^2$$

It generates $R^2 = 0.96$, which is very high and the p-value is $0.015 < 0.05$. The second subset (SO) consisting of compounds 20-32 are utilized to construct models based on a similar approach taken previously. Subset SO has 2 heterogeneous sub-groups. While the first one comprises compounds 20, 21, 22, 23, 27, 28, 30 and 32, the second one consists of compounds 24, 25, 26, 29 and 31. For the sub-groups 1 and 2, we defined a new variable called K as follows:

$$K = \frac{\sqrt{MV}}{I}$$

Then, a linear regression method is conducted to construct a model between pIC_{50} and *K*

for sub-group 1 consisting of compounds 20, 21, 22, 23, 27, 28, 30 and 32:

$$\mathrm{pIC_{50}} = -5.839 + 3.364 * K$$

The resulting model leads to $R^2 = 0.98$, which is very high and the *p*-value is 0.00 < 0.05. The sub-group 2 (24, 25, 26, 29 and 31) leads to a model defined by

$$\mathrm{pIC_{50}} = 77.85 - 334.1 * Y + 328.7 * K^2$$

Its $R^2 = 0.78$ is high and the *p*-value is 0.025 < 0.05. For the subset SO_2 (compounds 33–61), four sub-groups are generated. For the first sub-group (37, 38, 39, 43, 44, 45, 47, 49, 54, 56 and 59), the constructed model in terms of K is given as follows:

$$K = \frac{\sqrt{MV}}{I}$$

Then, linear regression is constructed between $\mathrm{pIC_{50}}$ and K as follows:

$$\mathrm{pIC_{50}} = -27.817 + 14.405 * K$$

Its $R^2 = 0.78$ is high and the *p*-value is 0.025 < 0.05. For the sub-group 2 (33, 36, 41, 42, 51, 52, 53, 55, 58 and 60), the constructed model is given by:

$$\mathrm{pIC_{50}} = 1.61 * \exp(-9.666 * K)$$

It leads to $R^2 = 0.65$ and the *p*-value is 0.006 < 0.05. For sub-group 3 (34, 35, 40, 46 and 61), the model is given by:

$$\mathrm{pIC_{50}} = -3.548 + 3.095 * K$$

It leads to $R^2 = 0.82$ and the *p*-value is 0.034 < 0.05. For sub-group 4 (48, 50 and 57), the model is given by:

$$\mathrm{pIC_{50}} = -623.5 + 2654 * Z - 2811 * K^2$$

The constructed model has $R^2 = 0.92$, which is very high and the *p*-value is 0.044 < 0.05. Two software, which are SPSS 24.0 and Mat Lab 7.9, are used to construct all the models

Discussion for Statistical Analysis

We examined 61 compounds in the gas phase that are classified as three groups, which are called subsets S, SO and SO_2, according to the atoms and groups connected in the X position. Even though they are split into three groups from the chemical point of view, we run a statistical model called Linear Discriminant Analysis to verify this classification. Hence, the results suggest that the classification into three groups is validated. On the other hand, the compounds in each group, however, exhibit heterogeneous characteristics that result in two or more than two heterogeneous sub-groups. Therefore, each sub-group of compounds is modelled separately. While $\frac{\Delta E}{I}$ ratio accounts for $\sqrt{\mathrm{pIC_{50}}}$ for S (subset S), $\frac{I+DM}{EN*Electrophily}$ ratio accounts for $\sqrt{\mathrm{pIC_{50}}}$ for SO (subset SO) with the highest R^2 coefficient values. On the other hand, the descriptor called TMC accounts for $\mathrm{pIC_{50}}$ SO_2 (subset SO_2), $\frac{\Delta E}{I}$ ratio accounts for $\mathrm{pIC_{50}}$ with the highest R^2 coefficient values in the gas phase. On the other hand, the ratio, $\frac{\sqrt{MV}}{I}$, accounts for $\mathrm{pIC_{50}}$ with the highest R^2 coefficient values for S, SO, and SO_2, respectively when the water phase is used.

In conclusion, although the dependent variable, called the $\mathrm{pIC_{50}}$ in the water phase, is accounted for only a single ratio called, $\frac{\sqrt{MV}}{I}$, the dependent variable named the $\mathrm{pIC_{50}}$ in the gas phase is accounted for two different ratios, called, $\frac{\Delta E}{I}$ and $\frac{I+DM}{EN*Electrophily}$, respectively concerning which group is under consideration.

The discussion on corrosion inhibition is speculative and based on structural analogies with known inhibitors. While the presence of heteroatoms (N, O, S) and π-systems supports potential inhibitor activity, experimental validation is required to confirm adsorption behaviour and inhibition efficiency. Recent studies highlight the importance of synergistic effects and adsorption mechanisms for biologically active molecules in corrosion protection [79, 80]. Therefore, this section should be considered as a theoretical proposal for future experimental investigation.

Conclusions

In this study, some quantum chemical calculations were performed, and investigated electronic structure parameters such as frontier orbital energies, energy gap, ionization potential, chemical hardness, softness, dipole moment, electronegativity, and relationship of $\mathrm{pIC_{50}}$ with these parameters for the 2-amino-6-aryl-sulfonyl benzonitrile derivatives (1-61). These compounds examined as three series: compounds 1-19: Subset S, compounds 20-32: Subset SO and compounds 33-61: Subset SO_2, according to the atoms and groups connected in the X position. These electronic structure parameters have been found

by using Gaussian 09 (Revision A.02) software with B3LYP/6-311G(d,p) basic set for gas and water phases of molecules, and discussed the relationship between these results with reaction efficiency. In addition to electronic structure parameters, statistical analysis of molecules is discussed.

Even though each group is assumed to be homogenous, we found that each group composes of heterogeneous subgroups that generate different models with different quantum descriptors. Hence, the subgroups of the compounds need to be treated separately when statistical modelling is conducted.

According to the study results, the three molecules with the highest pIC_{50} rank can be summarized as: According to E_{HOMO} values, 13 > 12 > 14 for the gas phase and 13 > 7 > 9 for the solvent phase of subset S, 27 > 26 > 30 for the gas phase and 30 > 26 > 27 for the solvent phase of subset SO, and 50 > 49 > 53 for the gas phase and 52 > 40 > 48 for the solvent phase of subset SO_2; according to energy gap (ΔE) values, 2 > 15 > 9 for the gas and 15 > 2 > 18 for the solvent phase of subset S, 24 > 21 > 20 for the gas phase and 30 > 24 > 26 for the solvent phase of subset SO, and 50 > 53 > 49 for the gas phase and 50 > 48 > 53 for the solvent phase of subset SO_2; according to ionization potential (I) values, 15 > 2 > 18 for the gas and solvent phases of subset S, 20 > 21 > 29 for the gas phase and 20 > 29 > 23 for the solvent phase of subset SO, and 34 > 61 > 60 for the gas phase and 34 > 36 > 60 for the solvent phase of subset SO_2; according to the electronegativity (χ) values, 15 > 2 > 18 for the gas and 15 > 2 > 16 for the solvent phases of subset S, 20 > 21 > 29 for the gas phase and 20 > 29 > 23 for the solvent phase of subset SO, and 34 > 60 > 61 for the gas phase and 34 > 36 > 37 for the solvent phase of subset SO_2. According to the quantum chemical parameter results, the activity and inhibitor efficiency rankings for the gas and solvent phases are seen to be almost similar, despite minor differences (Table 4).

The two different phases for 61 compounds, which are called gas and water, have been utilized to account for the relationship between pIC_{50} and the descriptor variables of those compounds. All relationships that are constructed are nonlinear. Even though compounds are classified into three groups, each group is not homogenous by itself. In other words, each group consists of heterogeneous subgroups that require constructing different models. For example, when S (subset S) in the gas phase is considered, it has three heterogeneous subgroups. Thus, pIC_{50} for each group is accounted for using descriptor variables. Interestingly, the same ratio, called $\frac{\Delta E}{I}$, in each subgroup appears to be a descriptor variable. On the other hand, SO_2 (subset SO_2) has three subgroups. pIC_{50} for each group is accounted for using different descriptor variables. While *MAC* is a descriptor variable for one subgroup, the ratio, called $\frac{\Delta E}{I}$, is utilized for the other two subgroups. Similar results are obtained for the compounds in the water phase.

In summary, this study successfully integrates DFT calculations with statistical modelling to identify key quantum descriptors influencing the anti-HIV activity of 2-amino-6-arylsulfonylbenzonitrile derivatives. The models demonstrate high explanatory power through internal validation; however, external validation on independent compounds is recommended to confirm predictive robustness. Additionally, while the corrosion inhibition potential is discussed theoretically, experimental studies are necessary to substantiate these claims. Future work should also explore explicit solvation models and mechanistic studies to further elucidate the structure-activity relationships.

Acknowledgments

The computers used for quantum chemical calculations were allocated by the Erciyes University data centre.

Table-4: The most active compounds according to some quantum chemical parameter results for the gas and water phases.

	Subset S		Subset SO		Subset SO_2	
Parameter	**Gas**	**Water**	**Gas**	**Water**	**Gas**	**Water**
E_{HOMO}	13 > 12 > 14	13 > 7 > 9	27 > 26 > 30	30 > 26 > 27	50 > 49 > 53	52 > 40 > 48
ΔE	2 > 15 > 9	15 > 2 > 18	24 > 21 > 20	30 > 24 > 26	50 > 53 > 49	50 > 48 > 53
I	15 > 2 > 18	15 > 2 > 18	20 > 21 > 29	20 > 29 > 23	34 > 61 > 60	34 > 36 > 60
χ	15 > 2 > 18	15 > 2 > 16	20 > 21 > 29	20 > 29 > 23	34 > 60 > 61	34 > 36 > 37
DM	12 > 13 > 14	12 > 13 > 14	26 > 27 > 28	26 > 27 > 28	48 > 49 > 51	48 > 51 > 49

References

1. HIV.Gov, Global HIV Data and Statistics, Available from, https://www.hiv.gov/hiv-basics/overview/data-and-trends/global-statistics, (2023).
2. N. Azzman, M. S. A. Gill, S. S. Hassan, F. Christ, Z. Debyser, W. A. S. Mohamed and N. Ahemad, Pharmacological Advances in Anti-Retroviral Therapy for Human Immunodeficiency Virus-1 Infection: A Comprehensive Review, *Rev. Med. Virol.*, ***34***, 2529 (2024). https://doi.org/10.1002/rmv.2529.
3. R. Hua, J. P. Doucet, M. Delamar and R. Zhang, QSAR Models for 2-Amino-6-Arylsulfonylbenzonitriles and Congeners HIV-1 Reverse Transcriptase Inhibitors Based on Linear and Nonlinear Regression Methods, *Eur. J. Med. Chem.*, ***44***, 2158 (2009). https://doi.org/10.1016/j.ejmech.2008.10.021.
4. S. X. Gu, T. Xiao, Y. Y. Zhu, and F. E. Chen, Recent Progress in HIV-1 Inhibitors Targeting the Entrance Channel of HIV-1 Non-Nucleoside Reverse Transcriptase Inhibitor Binding Pocket, *European J. Med. Chem.*, ***174***, 277 (2019). https://doi.org/10.1016/j.ejmech.2019.04.054.
5. J. H. Chan, J. S. Hong, R. N. Hunter, G. F. Orr, J. R. Cowan, D. B. Sherman, S. M. Sparks, B. E. Reitter, C. W. Andrews, R. J. Hazen, M. St Clair, L. R. Boone, R. G. Ferris, K. L. Creech, G. B. Roberts, S. A. Short, K. Weaver, R. J. Ott, J. Ren, A. Hopkins, D. I. Stuart and D. K. Stammers, 2-Amino-6-Arylsulfonylbenzonitriles as Non-Nucleoside Reverse Transcriptase Inhibitors of HIV-1, *J. Med. Chem.*, ***44***, 1866 (2001). https://pubs.acs.org/doi/10.1021/jm0004906.
6. K. Roy and J. T. Leonard, QSAR Modelling of HIV-1 Reverse Transcriptase Inhibitor 2-Amino-6-Arylsulfonylbenzonitriles and Congeners Using Molecular Connectivity and E-State Parameters, *Bioorg. Med. Chem.*, ***12***, 745 (2004). https://doi.org/10.1016/j.bmc.2003.11.009.
7. R. Hu, F. Barbault, M. Delamar and R. Zhang, Receptor and Ligand-Based 3D-QSAR Study for a Series of Non-Nucleoside HIV-1 Reverse Transcriptase Inhibitors, *Bioorg. Med. Chem.*, ***17***, 2400 (2009). https://doi.org/10.1016/j.bmc.2009.02.003.
8. J. R. Pinheiro, M. Bitencourt, E. F. F. da Cunha, T. C. Ramalho and M. P. Freitas, Novel Anti-HIV Cyclotriazadisulfonamide Derivatives as Modeled by Ligand and Receptor-Based Approaches, *Bioorg. Med. Chem*., ***16***, 1683 (2008). https://doi.org/10.1016/j.bmc.2007.11.020.
9. R. Sabet and M. Sabet, Application of Substituent Electronic Descriptors QSAR Model of 2-Amino-6-Arylsulfonylbenzonitriles as HIV-1 Reverse Transcriptase Inhibitors Based on The MOLMAP Approach, *Asian J. App. Chem. Res.*, ***1***, 1 (2018). https://doi.org/10.9734/ajacr/2018/v1i29617.
10. R. D. Cramer, D. E. Patterson and J. D. Bunce, Comparative Molecular Field Analysis (CoMFA). 1. Effect of Shape on Binding of Steroids to Carrier Proteins, *J. Am. Chem. Soc.*, ***110***, 5959 (1988). https://doi.org/10.1021/ja00226a005.
11. T. Aoyama, Y. Suzuki and H. Ichikawa, Neural Networks Applied to Structure-Activity Relationships, *J. Med. Chem.*, ***33***, 905 (1990). https://doi.org/10.1021/jm00165a004.
12. T. Aoyama, Y. Suzuki and H. Ichikawa, Neural Networks Applied to Pharmaceutical Problems. III. Neural Networks Applied to Quantitative Structure-Activity Relationship (QSAR) Analysis, *J. Med. Chem.*, ***33***, 2583 (1990). https://doi.org/10.1021/jm00171a037.
13. X. J. Yao, A. Panaye, J. P. Doucet, R. S. Zhang, H. F. Chen, M. C. Liu, Z. D. Hu and B. T. Fan, Comparative Study of QSAR/QSPR Correlations Using Support Vector Machines, Radial Basis Function Neural Networks, and Multiple Linear Regression, *J. Chem. Inf. Comput. Sci.*, ***44***, 1257 (2004). https://doi.org/10.1021/ci049965i.
14. A. Szczurek and M. Maciejewska, Recognition of Benzene, Toluene and Xylene Using TGS Array Integrated with Linear and Non-Linear Classifier, *Talanta*, ***64***, 609 (2004). https://doi.org/10.1016/j.talanta.2004.03.036.
15. X. Ding, D. Kang, L. Sun, P. Zhan and X. Liu, Combination of 2D and 3D-QSAR Studies on DAPY and DANA Derivatives as Potent HIV-1 NNRTIs, *J. Mol. Struct*., ***1249***, 131603 (2022). https://doi.org/10.1016/j.molstruc.2021.131603.
16. X. J. Yao, A. Panaye, J. P. Doucet, R. S. Zhang, H. F. Chen, M. C. Liu, Z. D. Hu and B. T. Fan, Comparative Study of QSAR/QSPR Correlations Using Support Vector Machines, Radial Basis Function Neural Networks, and Multiple Linear Regression, *J. Chem. Inf. Comp. Sci.*, ***44***, 1257 (2004). https://doi.org/10.1021/ci049965i
17. R. Hu, F. Barbault, M. Delamar and R. Zhang, Receptor- and Ligand-Based 3D-QSAR Study for a Series of Non-Nucleoside HIV-1 Reverse Transcriptase Inhibitors, *Bioorg. Med. Chem.*, ***17***, 2400 (2009). https://doi.org/10.1016/j.bmc.2009.02.003

18. M. J. Frisch, G. W. Trucks, H. B. Schlegel, G. E. Scuseria, M. A. Robb, J. R. Cheeseman, G. Scalmani, V. Barone, G. A. Petersson, H. Nakatsuji, X. Li, M. Caricato, A. Marenich, J. Bloino, B. G. Janesko, R. Gomperts, B. Mennucci, H. P. Hratchian, J. V. Ortiz, A. F. Izmaylov, J. L. Sonnenberg, D. Williams-Young, F. Ding, F. Lipparini, F. Egidi, J. Goings, B. Peng, A. Petrone, T. Henderson, D. Ranasinghe, V. G. Zakrzewski, J. Gao, N. Rega, G. Zheng, W. Liang, M. Hada, M. Ehara, K. Toyota, R. Fukuda, J. Hasegawa, M. Ishida, T. Nakajima, Y. Honda, O. Kitao, H. Nakai, T. Vreven, K. Throssell, J. A. Montgomery, Jr., J. E. Peralta, F. Ogliaro, M. Bearpark, J. J. Heyd, E. Brothers, K. N. Kudin, V. N. Staroverov, T. Keith, R. Kobayashi, J. Normand, K. Raghavachari, A. Rendell, J. C. Burant, S. S. Iyengar, J. Tomasi, M. Cossi, J. M. Millam, M. Klene, C. Adamo, R. Cammi, J. W. Ochterski, R. L. Martin, K. Morokuma, O. Farkas, J. B. Foresman and D. J. Fox, *Gaussian 09, Revision A.02, Gaussian Inc*., Wallingford CT (2016).
19. M. Saracoglu, Z. Kokbudak, Z. Çimen and F. Kandemirli, Synthesis and DFT Quantum Chemical Calculations of Novel Pyrazolo[1,5-C]Pyrimidin-7(1*H*)-One Derivatives, *J. Chem. Soc. Pakistan*, ***41***, 479 (2019).
20. Z. Kökbudak, M. Saracoglu, S. Akkoç, Z. Çimen, M. I. Yilmazer and F. Kandemirli, Synthesis, Cytotoxic Activity and Quantum Chemical Calculations of New 7-Thioxopyrazolo[1,5-F]Pyrimidin-2-One Derivatives, *J. Mol. Struct.*, ***1202***, 127261 (2020). https://doi.org/10.1016/j.molstruc.2019.127261.
21. M. A. Amin, M. Saracoglu, N. El-Bagoury, T. Sharshar, M. M. Ibrahim, J. Wysocka, S. Krakowiak and J. Ryl, Microstructure and Corrosion Behaviour of Carbon Steel and Ferritic and Austenitic Stainless Steels in NaCl Solutions and the Effect of *p*-Nitrophenyl Phosphate Disodium Salt, *Int. J. Electrochem. Sci.*, ***11***, 10029 (2016). https://doi.org/10.20964/2016.12.17.
22. M. Saracoglu, Z. Kokbudak, M. I. Yilmazer and F. Kandemirli, Synthesis and DFT Studies of Pyrimidin-1(2*H*)-ylaminofumarate Derivatives, *J. Chem. Soc.*, Pakistan, ***42***, 746 (2020). https://doi.org/10.52568/000679/JCSP/42.05.2020.
23. M. A. Amin, O. A. Hazzazi, F. Kandemirli and M. Saracoglu, Inhibition Performance and Adsorptive Behaviour of Three Amino Acids on Cold Rolled Steel in 1.0 M HCl-Chemical, Electrochemical and Morphological Studies, *Corrosion*, ***68***, 688 (2012). https://doi.org/10.5006/0506.
24. F. Kandemirli, M. Saracoglu, G. Bulut, E. Ebenso, T. Arslan and A. Kayan, Synthesis, Theoretical Study on Zinc (II) and Nickel (II) Complexes of 5-Methoxyisatin 3-[N-(4-Chlorophenyl) Thiosemicarbazone], *J. Mat. Fund. Sci.*, ***44***, 35 (2012). https://doi.org/10.5614/itbj.sci.2012.44.1.4.
25. K. S. M. Ferigita, M. G. K. AlFalah, M. Saracoglu, Z. Kokbudak, S. Kaya, M. O. A. Alaghani and F. Kandemirli, Corrosion Behaviour of New Oxo-Pyrimidine Derivatives on Mild Steel in Acidic Media: Experimental, Surface Characterization, Theoretical, and Monte Carlo Studies, *App. Surf. Sci. Adv.*, ***7***, 100200 (2022). https://doi.org/10.1016/j.apsadv.2021.100200.
26. M. Saracoglu, M. I. A. Elusta, S. Kaya, C. Kaya and F. Kandemirli, Quantum Chemical Studies on the Corrosion Inhibition of $Fe_{78}B_{13}Si_9$ Glassy Alloy in Na_2SO_4 Solution of Some Thiosemicarbazone Derivatives, *Int. J. Electrochem. Sci.*, ***13***, 8241 (2018). https://doi.org/10.20964/2018.08.74.
27. F. Kandemirli, M. Saracoglu, M. A. Amin, M. A. Basaran and C. D. Vurdu, The Quantum Chemical Calculations of Serine, Therionine and Glutamine, *Int. J. Electrochem. Sci.*, ***9***, 7 3819 (2014).
28. A. Tazouti, M. Galai, R. Touir, M. E. Touhami, A. Zarrouk, Y. Ramli, M. Saracoglu, S. Kaya, F. Kandemirli and C. Kaya, Experimental and Theoretical Studies for Mild Steel Corrosion Inhibition in 1.0 M HCl by Three New Quinoxalinone Derivatives, *J. Mol. Liq.*, ***221,*** 815 (2016). https://doi.org/10.1016/j.molliq.2016.03.083.
29. K. S. M. Ferigita, M. Saracoglu, M. G. K. AlFalah, M. I. Yilmazer, Z. Kokbudak, S. Kaya and F. Kandemirli, Corrosion Inhibition of Mild Steel in Acidic Media Using New Oxo-Pyrimidine Derivatives: Experimental and Theoretical Insights, *J. Mol. Struc.*, ***1284***, 135361 (2023). https://doi.org/10.1016/j.molstruc.2023.135361.
30. M. G. K. AlFalah, K. S. M. Freigita, M. I. Yilmazer, M. Saracoglu, Z. Kokbudak and F. Kandemirli, Corrosion Inhibition Potential of New Oxo-Pyrimidine Derivative on Mild Steel in Acidic Solution: Experimental and Theoretical Approaches, *J. Mol. Struc.*, ***1315***, 138773 (2024). https://doi.org/10.1016/j.molstruc.2024.138773.

31. B. Saima, A. Khan, R. U. Nisa, T. Mahmood and K. Ayub, Theoretical Insights into Thermal Cyclophanediene to Dihydropyrene Electrocyclic Reactions, a Comparative Study of Woodward Hoffmann Allowed and Forbidden Reactions, *J. Mol. Model.*, ***22***, 81 (2016). https://doi.org/10.1007/s00894-016-2948-6.
32. M. Saracoglu, Z. Kokbudak, E. Yalcin and F. Kandemirli, Synthesis and DFT Quantum Chemical Calculations of 2-Oxopyrimidin-1(2*H*)-yl-Thiourea and Urea Derivatives, *J. Chem. Soc. Pakistan*, ***41***, 841 (2019).
33. M. Saracoglu, S. G. Kandemirli, A. Başaran, H. Sayiner and F. Kandemirli, Investigation of Structure-Activity Relationship Between Chemical Structure and CCR5 Anti-HIV-1 Activity in a Class of 1-[N-(Methyl)-N-(Phenylsulfonyl)Amino]-2-(Phenyl)-4-[4-(Substituted)Piperidin-1-yl]Butane Derivatives: The Electronic-Topological Approach, *Curr. HIV Res.*, ***9***, 300 (2011). http://dx.doi.org/10.2174/157016211797635964.
34. M. Saracoglu, F. Kandemirli, M. A. Amin, C. D. Vurdu, M. S. Cavus and G. Sayıner, *The Quantum Chemical Calculations of Some Thiazole Derivatives, Proc. 3rd Int. Conf. Comp. Sci. Technol. (ICCST-3)*, Published by Atlantis Press, ***5***, p. 149 (2015). https://doi.org/10.2991/iccst-15.2015.29.
35. M. G. L. Annaamalai, G. Maheswaran, N. Ramesh, C. Kamal, G. Venkatesh and P. Vennila, Investigation of Corrosion Inhibition of Welan Gum and Neem Gum on Reinforcing Steel Embedded in Concrete, *Int. J. Electrochem. Sci.*, ***13***, 9981 (2018). https://doi.org/10.20964/2018.10.41.
36. G. Venkatesh, C. Kamal, P. Vennila, S. Kaya, M . G. L. Annaamalai and B. El Ibrahimi, Sustainable Corrosion Inhibitor for Steel Embedded in Concrete by Guar Gum: Electrochemical and Theoretical Analyses, *Appl. Surf. Sci. Adv.*, ***12***, 100328 (2025). https://doi.org/10.1016/j.apsadv.2022.100328.
37. N. Er-rahmany, M. Nounah, S. Yaqouti, A. Nounah, R. Touir and E. H. El Kafssaoui, Quinoxaline Derivatives as Corrosion Inhibitors: Development of Predictive Machine Using Partial Least Squares and Random Forest (PLS/RF) Models Based on Quantitative Structure-Activity Relationship (QSAR), *Next Res.*, ***2***, 100148 (2025). https://doi.org/10.1016/j.nexres.2025.100148.
38. R. Farahati, S. M. Mousavi-Khoshdel, A. Ghaffarinejad and H. Behzadi, Experimental and Computational Study of Penicillamine Drug and Cysteine as Water-Soluble Green Corrosion Inhibitors of Mild Steel, *Prog. Org. Coat.*, ***142***, 105567 (2020). https://doi.org/10.1016/j.porgcoat.2020.105567.
39. N. Palaniappan, J. Alphonsa, I. S. Cole, K. Balasubramanian and I. G. Bosco, Rapid Investigation Expiry Drug Green Corrosion Inhibitor on Mild Steel in NaCl Medium, *Mat. Sci. Eng. B.*, ***249***, 114423 (2019). https://doi.org/10.1016/j.mseb.2019.114423.
40. Q. H. Zhang, B. S. Hou, Y. Y. Li, Y. Lei, X. Wang, H. F. Liu and G.A. Zhang, Two Amino Acid Derivatives as High Efficient Green Inhibitors for the Corrosion of Carbon Steel in CO_2-Saturated Formation Water, *Corr. Sci.*, ***189***, 109596 (2021). https://doi.org/10.1016/j.corsci.2021.109596.
41. N. Al-Akhras and Y. Mashaqbeh, Potential Use of Eucalyptus Leaves as Green Corrosion Inhibitor of Steel Reinforcement, *J. Build. Eng.*, ***35***, 101848 (2021). https://doi.org/10.1016/j.jobe.2020.101848.
42. K. Haruna, T. A. Saleh and M. A. Quraishi, Expired Metformin Drug as Green Corrosion Inhibitor for Simulated Oil/Gas Well Acidizing Environment, *J. Mol. Liq.*, ***315***, 113716 (2020). https://doi.org/10.1016/j.molliq.2020.113716.
43. P. Geethamani and P. K. Kasthuri, The Inhibitory Action of Expired Asthalin Drug on the Corrosion of Mild Steel in Acidic Media: A Comparative Study, *J. Taiwan Inst. Chem. E.*, ***63***, 490-499 (2016). https://doi.org/10.1016/j.jtice.2016.03.008.
44. P. Singh, D. S. Chauhan, S. S. Chauhan, G. Singh and M. A. Quraishi, Chemically Modified Expired Dapsone Drug as Environmentally Benign Corrosion Inhibitor for Mild Steel in Sulphuric Acid Useful for Industrial Pickling Process, *J. Mol. Liq.*, ***286***, 110903 (2019). https://doi.org/10.1016/j.molliq.2019.110903.
45. K. F. Khaled, Studies of Iron Corrosion Inhibition Using Chemical, Electrochemical and Computer Simulation Techniques, *Electrochim. Acta*, ***55***, 6523 (2010). https://doi.org/10.1016/j.electacta.2010.06.027.
46. M. J. S. Dewar and W. Thiel, Ground States of Molecules. 38. The MNDO Method. Approximations and Parameters, *J. Am. Chem. Soc.*, ***99***, 4899 (1977). https://doi.org/10.1021/ja00457a004.

47. R. G. Pearson, Hard and Soft Acids and Bases—the Evolution of a Chemical Concept, *Coord. Chem. Rev*., ***100,*** 403 (1990). https://doi.org/10.1016/0010-8545(90)85016-L.
48. L. Pauling, *The Nature of the Chemical bond, Cornell University Press*, New York, USA (1960).
49. R. G. Parr and R. G. Pearson, Absolute Hardness: Companion Parameter to Absolute Electronegativity, *J. Am. Chem. Soc*., ***105***, 7512 (1983). https://doi.org/10.1021/ja00364a005.
50. P. K. Chattaraj, U. Sarkar and D. R. Roy, Electrophilicity Index, *Chem. Rev*., ***106***, 2065 (2006). https://doi.org/10.1021/cr040109f.
51. E. E. Ebenso, M. M. Kabanda, T. Arslan, M. Saracoglu, F. Kandemirli, L. C. Murulana, A. K. Singh, S. K. Shukla, B. Hammouti, K. F. Khaled, M. A. Quraishi, I. B. Obot and N. O. Edd, Quantum Chemical Investigations on Quinoline Derivatives as Effective Corrosion Inhibitors for Mild Steel in Acidic Medium, *Int. J. Electrochem. Sci*., ***7***, 5643 (2012).
52. A. Y. Musa, A. H. Kadhum, A. B. Mohamad, A. B. Rohoma and H. Mesmari, Electrochemical and Quantum Chemical Calculations on 4,4-Dimethyloxazolidine-2-Thione as Inhibitor for Mild Steel Corrosion in Hydrochloric Acid, *J. Mol. Struct*., ***969***, 233 (2010). https://doi.org/10.1016/j.molstruc.2010.02.051.
53. K. F. Khaleda and M. M. Al-Qahtani, The Inhibitive Effect of Some Tetrazole Derivatives Towards Al Corrosion in Acid Solution: Chemical, Electrochemical and Theoretical Studies, *Mater. Chem. Phys.*, ***113***, 150 (2009). https://doi.org/10.1016/j.matchemphys.2008.07.060.
54. H. Luo, Y. C. Guan and K. N. Han, Corrosion Inhibition of a Mild Steel by Aniline and Alkylamines in Acidic Solutions, *Corrosion*, ***54***, 721 (1998). https://doi.org/10.5006/1.3284891.
55. S. Martinez and I. Štagljar, Correlation Between the Molecular Structure and the Corrosion Inhibition Efficiency of Chestnut Tannin in Acidic Solutions, *J. Mol. Struct.: THEOCHEM*, ***640***, 167 (2003). https://doi.org/10.1016/j.theochem.2003.08.126.
56. R. G. Pearson, Hard and Soft Acids and Bases, *Survey Prog. Chem.*, ***5***, 1 (1969). https://doi.org/10.1016/B978-0-12-395706-1.50007-8.
57. M. M., Solomon S. A. Umoren, I. I. Udosoro and A. P. Udoh, Inhibitive and Adsorption Behaviour of Carboxymethyl Cellulose on Mild Steel Corrosion in Sulphuric Acid Solution, *Corros. Sci.*, ***52***, 1317 (2010). https://doi.org/10.1016/j.corsci.2009.11.041.
58. A. Rauk, *Orbital Interaction Theory of Organic Chemistry*, *Wiley & Sons*, New York, USA (2001). https://doi.org/10.1002/0471220418.ch3.
59. M. B. Manaa, N. Issaoui, N. Bouaziz and A. B. Lamine, Combined Statistical Physics Models and DFT Theory to Study the Adsorption Process of Paprika Dye on TiO_2 for Dye Sensitized Solar Cells, *J. Mater. Res. Technol*., ***9-2***, 1175 (2020). https://doi.org/10.1016/j.jmrt.2019.11.045
60. M. Khodiev, U. Holikulov, A. Jumabaev, N. Issa oui, L. N. Lvovich, O. M. Al-Dossary and L. G. Bousiakoug, Solvent Effect on the Self-Association of the 1,2,4-Triazole: A DFT Study, *J. Mol. Liq.*, ***382***, 121960 (2023). https://doi.org/10.1016/j.molliq.2023.121960
61. N. O. Obi-Egbedi, I. B. Obot and M. I. El-Khaiary, Quantum Chemical Investigation and Statistical Analysis of the Relationship Between Corrosion Inhibition Efficiency and Molecular Structure of Xanthene and Its Derivatives on Mild Steel in Sulphuric Acid, J. *Mol. Struct.*, ***1002***, 86 (2011). https://doi.org/10.1016/j.molstruc.2011.07.003.
62. M. Djenane, S. Chafaa, N. Chafai, R. Kerkour and A. Hellal, Synthesis, Spectral Properties and Corrosion Inhibition Efficiency of New Ethyl Hydrogen [(Methoxyphenyl) (Methylamino) Methyl] Phosphonate Derivatives: Experimental and Theoretical Investigation, *J. Mol. Struct.*, ***1175***, 398 (2019). https://doi.org/10.1016/j.molstruc.2018.07.087.
63. J. Bhawsar, P. Jain, M. G. Valladares-Cisneros, C. Cuevas-Arteaga and M. R. Bhawsar, Quantum Chemical Assessment of Two Natural Compounds: Vasicine and Vasicinone as Green Corrosion Inhibitors, *Int. J. Electrochem. Sci.*, ***13***, 3200 (2018). https://doi.org/10.20964/2018.04.57.
64. I. B. Obot, N. O. Obi-Egbedi and A. O. Eseola, Anticorrosion Potential of 2-Mesityl-1H-Imidazo[4,5-F][1,10]Phenanthroline on Mild Steel in Sulfuric Acid Solution: Experimental and Theoretical Study, *Ind. Eng. Chem. Res*., ***50***, 2098 (2011). https://doi.org/10.1021/ie102034c.
65. I. B. Obot, N. O. Obi-Egbedi, E. E. Ebenso, A. S. Afolabi and E. E. Oguzie, Experimental, Quantum Chemical Calculations, and Molecular Dynamic Simulations Insight into the Corrosion Inhibition Properties of 2-(6-Methylpyridin-2-yl)Oxazolo[5,4-F][1,10]Phenanthroline on Mild Steel, *Res. Chem. Intermed.*, ***39***, 1927 (2013). https://doi.org/10.1007/s11164-012-0726-3.

66. R. G. Parr and P. K. Chattaraj, Principle of Maximum Hardness, *J. Am. Chem. Soc.*, ***113***, 1854 (1991). https://doi.org/10.1021/ja00005a072.
67. D. Bhattacharjee, T. K. Devi, R. Dabrowski and A. Bhattacharjee, Birefringence, Polarizability Order Parameters and DFT Calculations in The Nematic Phase of Two Bent-Core Liquid Crystals and Their Correlation, *J. Mol. Liq.*, ***272***, 239 (2018). https://doi.org/10.1016/j.molliq.2018.09.052.
68. R. G. Pearson, The Principle of Maximum Hardness, *Acc. Chem. Res.*, ***26***, 250 (1993). https://doi.org/10.1021/ar00029a004.
69. R. G. Pearson, Absolute Electronegativity and Hardness Correlated with Molecular Orbital Theory, *Proc. Nat. Acad. Sci. USA*, ***83***, 8440 (1986). https://doi.org/10.1073/pnas.83.22.8440.
70. M. M. Ibrahim, G. A. M. Mersal, A. M. Fallatah, M. Saracoglu, F. Kandemirli, S. Alharthi, S. Szunerits, R. Boukherroub, J. Ryl and M. A. Amin, Electrochemical, Theoretical and Surface Physicochemical Studies of The Alkaline Copper Corrosion Inhibition by Newly Synthesized Molecular Complexes of Benzenediamine and -Tetraamine with Π Acceptor, *J. Mol. Liq.*, ***320***, 114386 (2020). https://doi.org/10.1016/j.molliq.2020.114386.
71. C. Verma, M. A. Quraishi, K. Kluza, M. Makowska-Janusik, L. O. Olasunkanmi and E. E. Ebenso, Corrosion Inhibition of Mild Steel in 1 M HCl by D-Glucose Derivatives of Dihydropyrido [2,3-D:6,5-D'] Dipyrimidine-2, 4, 6, 8(1H, 3H, 5H, 7H)-Tetraone, *Sci. Rep.*, ***7***, 44432 (2017). https://doi.org/10.1038/srep44432.
72. G. Gao and C. Liang, Electrochemical and DFT Studies of β-Amino-Alcohols as Corrosion Inhibitors for Brass, *Electrochim. Acta*, ***52***, 4554 (2007). https://doi.org/10.1016/j.electacta.2006.12.058.
73. M. Sahin, G. Gece, F. Karci and S. Bilgic, Experimental and Theoretical Study of The Effect of Some Heterocyclic Compounds on the Corrosion of Low Carbon Steel in 3.5% NaCl Medium, *J. Appl. Electrochem.*, ***38***, 809 (2008). https://doi.org/10.1007/s10800-008-9517-3.
74. M. A. Quraishi and R. Sardar, Hector Bases – a New Class of Heterocyclic Corrosion Inhibitors for Mild Steel in Acid Solutions, *J. Appl. Electrochem.*, ***33***, 1163 (2003). https://doi.org/10.1023/B:JACH.0000003865.08986.fb.
75. M. Shahraki, M. Dehdab and S. Elmi, Comparative Theoretical and Experimental Studies on Corrosion Inhibition of Aluminum in Acidic Media by the Anti-Biotics Drugs, *J. Taiwan Inst. Chem. Eng.*, ***62***, 313 (2016). https://doi.org/10.1016/j.jtice.2016.02.010.
76. A. Singh, Y. Lin, M. Quraishi, L. Olasunkanmi, O. Fayemi, Y. Sasikumar, B. Ramaganthan, I. Bahadur, I. Obot, A. Adekunle, M. Kabanda and E. E. Ebenso, Porphyrins as Corrosion Inhibitors for N80 Steel in 3.5% NaCl Solution: Electrochemical, Quantum Chemical, QSAR and Monte Carlo Simulations Studies, *Molecules*, ***20***, 15122 (2015). https://doi.org/10.3390/molecules200815122.
77. G. Gece, The Use of Quantum Chemical Methods in Corrosion Inhibitor Studies, *Corros. Sci.*, ***50***, 2981 (2008). https://doi.org/10.1016/j.corsci.2008.08.043.
78. J. N. Murrell, S. F. Kettle and J. M. Tedder, *The Chemical Bond, John Wiley & Sons*, Chichester, UK (1985).
79. A. Ramalingam, N. Mustafa, W. J. Chng, M. Medimagh, S. Sambandam and N. Issaoui, 3-Chloro-3-Methyl-2,6-Diarylpiperidin-4-Ones as Anti-Cancer Agents: Synthesis, Biological Evaluation, Molecular Docking, and in Silico ADMET Prediction, *Biomolecules*, ***12(8)***, 1093 (2022). https://doi.org/10.3390/biom12081093
80. A. S. Kazachenko, N. Y. Vasilieva, O. Y. Fetisova, V. V. Sychev, E. V. Elsuf'ev, Y. N. Malyar, N. Issaoui, A. V. Miroshnikova, V. S. Borovkova, A. S. Kazachenko, Y. D. Berezhnaya, A. M. Skripnikov, D. V. Zimonin and V. A. Ionin, New Reactions of Betulin with Sulfamic Acid and Ammonium Sulfamate in the Presence of Solid Catalysts, *Biomass Convers. Biorefin.*, ***14***, 4245 (2024). https://doi.org/10.1007/s13399-022-02587-x